Biomass-burning derived particles from a wide variety of fuels: Part 1: Properties of primary particles

Crystal D. McClure[1], Christopher Y. Lim[2,%], David H. Hagan[2], Jesse H. Kroll[2], Christopher D. Cappa[1,3,*]

[1] Department of Civil and Environmental Engineering, University of California, Davis, CA 95616
[2] Department of Civil and Environmental Engineering, Massachusetts Institute of Technology, Cambridge, MA, USA
[3] Atmospheric Sciences Graduate Group, University of California, Davis, CA, USA 95616
[%] Now at Department of Chemistry, University of Toronto, Ontario, Canada

[*] To whom correspondence should be addressed: cdcappa@ucdavis.edu

ABSTRACT

Relationships between various optical, physical, and chemical properties of biomass combustion derived particles are characterized for particles produced from a wide range of fuels and burn conditions. The modified combustion efficiency (MCE), commonly used to parameterize biomass particle emissions and properties, is shown to generally have weak predictive capabilities, especially for more efficient combustion conditions. There is, however, a strong relationship between many intensive optical properties (e.g. single scatter albedo, Ångstrom absorption exponent, mass absorption efficiency) and the organic aerosol-to-black carbon ([OA]/[BC]) mass ratio over a wider range than previously considered (0.3 to 10^5). The properties of brown carbon (BrC, i.e. light absorbing organic carbon) also vary with [OA]/[BC]. The contribution of coating-induced enhancements (i.e. "lensing" effects) to absorption by black carbon are shown to be negligible for all conditions. The BC-OA mixing state varies strongly with [OA]/[BC]; the fraction of OA that is internally mixed with BC decreases with [OA]/[BC] while the relative amount of OA coated on BC increases. In contrast, there is little relationship between many OA bulk chemical properties and [OA]/[BC], with the O:C and H:C atomic ratios and the relative abundance of a key marker ion (m/z = 60, linked to levoglucosan) all showing no dependence on [OA]/[BC]. In contrast, both the organic nitrate fraction of OA and the OA volatility do depend on the [OA]/[BC]. Neither the total particle or BC-specific size distributions exhibit any clear dependence on the burn conditions or [OA]/[BC], although there is perhaps a dependence on fuel type. Overall, our results expand on existing knowledge to contribute new understanding of the properties of particles emitted from biomass combustion.

1 Introduction

While it is understood that both open and controlled biomass combustion are major sources of particles to the atmosphere (Andreae and Merlet, 2001), questions remain regarding the properties of the emitted particles, their relationship with combustion conditions and fuel type, and their atmospheric evolution. Particles emitted from biomass combustion impact the global radiation budget and contribute to poor air quality in impacted regions. The emitted primary particles are primarily composed of organic aerosol (OA) and black carbon (BC), in varying amounts, with trace inorganic species (Reid et al., 2005;McMeeking et al., 2009;Levin et al., 2010). Particle intensive properties are often compared against the modified combustion efficiency (MCE ~ $\Delta[CO_2]/(\Delta[CO]+ \Delta[CO_2])$), which provides a measure of the combustion efficiency of a burn. For example, various particle properties show some relationship with MCE, but often these relationships are weak, especially for more efficient combustion (higher MCE, corresponding typically to flaming conditions) (McMeeking et al., 2009;Liu et al., 2013;McMeeking et al., 2014). Understanding the diversity in the chemical, physical, and optical properties of the emitted particles is important for establishing the fire- or region-specific emissions and subsequent impacts.

The emitted OA from biomass combustion is somewhat light absorbing (Kirchstetter et al., 2004). Absorbing OA is commonly referred to as brown carbon (BrC), with properties that appear to depend on the fuel and combustion conditions (Saleh et al., 2014;Laskin et al., 2018), which affect particle organic composition (Jen et al., 2019). However, the properties of primary BrC absorption and, especially, understanding of the relationships between BrC absorption and other particle properties and burn conditions is only beginning to be unraveled. Additionally, it is established from theory and laboratory experiments that non-absorbing coatings on black carbon and other strongly absorbing particles can enhance the absorption (commonly referred to as the "lensing" effect but more accurately termed here the coating-induced enhancement) (Fuller et al., 1999;Bond et al., 2006;Lack et al., 2009;Shiraiwa et al., 2010;Cappa et al., 2012). Yet, the extent to which coating-induced enhancements impact absorption by ambient particles or for mixed-component particles from complex sources, such as biomass burning, remains contentious (Cappa et al., 2012;Healy et al., 2015;Liu et al., 2015;Peng et al., 2016;Liu et al., 2017).

61   Here, we expand on current understanding of the relationships between various primary

62   particle properties and burn conditions by analyzing measurements of primary biomass burning

63   particles produced from combustion of a variety of fuel types, many of particular relevance to the

64   western U.S.. We demonstrate that various optical properties exhibit a strong relationship with the

65   [OA]/[BC] mass ratio, much stronger than their relationship with the MCE. We use the

66   measurements to quantify the individual contributions of BC, BrC and from internal mixing of BC

67   to the observed light absorption, and examine the variability in the properties of BrC specifically.

68   We uniquely characterize the mixing state of BC and OA, and how mixing state vary between

69   individual burns and depend on the mean properties of the emitted particles. We characterize the

70   variability of OA-specific properties, including OA volatility, bulk chemical composition

71   (characterized by the O:C and H:C atomic ratio, and the presence of key marker ions), and,

72   uniquely, the relative abundance of organic nitrate species. We also examine the variability in the

73   emitted particle size distribution, both for the total particles and for the BC particles specifically.

74   Some of our analysis serves to support and extend previously determined relationships by

75   considering a wider range of conditions, while other aspects are unique to this study. These

76   observations provide a foundation for understanding and interpretation of experiments on the

77   influence of photochemical aging on biomass particle properties, discussed in a related paper (Lim

78   et al., 2019).

79   **2   Methods**

80   All experiments were conducted during the Fire Influence on Regional to Global Environments

81   Experiment (FIREX) lab study, which took place at the Missoula Fire Sciences Lab in Missoula,

82   MT, USA during November, 2016. Numerous types of biomass were combusted in a large

83   chamber (12 x 12 x 19 m) and the smoke sampled to provide information on the physical, chemical,

84   and optical properties of the resulting smoke (i.e., particulate and gas emissions). The general fuels

85   types combusted included (exclusively or in combination): duff, dung, excelsior, straw, litter,

86   untreated lumber, rotten debris, woody debris, shrub, herbaceous, and canopy biomass. A complete

87   list of fuels and types is provided in **Table S1**, with further details available on the U.S. National

88   Oceanic   and   Atmospheric   Administration   (NOAA)   data   archive

89   (https://esrl.noaa.gov/csd/projects/firex/). All data used in this publication are also available on the

90   NOAA archive, with the processed data summarized in complementary data repository (Cappa et

91   al., 2019a).

92   Both "room" and "stack" burns were conducted, although here we include results only from

93   stack burns. During stack burns, the smoke was mixed with background room air and funneled up

94   a large cylindrical stack (2 m dia. x 15 m height) where it was sampled into a high-flow transfer

95   line at ca. 0.27 m^3/s. This flow rate corresponded to sampling approximately 10% of the stack

96   flow. Smoke was transferred to an adjacent room via the high-flow transfer line (residence time

97   ca. 2 s) where it was sub-sampled through a $PM_{2.5}$ cyclone and injected into a 0.25 m^3 Teflon

98   photochemical reaction chamber (the mini chamber). Details on the construction and operation of

99   the mini chamber can be found in (Lim et al., 2019). Here, we focus exclusively on the properties

100   of particles sampled prior to initiation of photochemical oxidation; results of the photochemical

101   oxidation experiments are discussed in a series of papers (Coggon et al., 2019;Lim et al., 2019).

102   In brief, prior to each burn, the chamber was flushed with clean air with a relative humidity (RH)

103   of approximately 40%. To fill the chamber, smoke was sub-sampled from the high-flow inlet and

104   injected across the entire burn (typically lasting for 10-20 minutes) or until the chamber

105   concentration reached a maximum. A suite of instruments sampled from the mini chamber at a

106   flow rate of approximately 6 lpm. This flow rate varied from burn to burn due to the exact suite of

107   instruments sampling. Clean makeup air was being injected simultaneously from a zero air

108   generator to equal the air being sampled out of the chamber. The sampled smoke was diluted by a

109   factor of ca. seven relative to the air in the high-flow inlet. Subsequent dilution after filling was

110   characterized by the decay of acetonitrile (ACN). Properties of the primary particles are averaged

111   over the 5-10 minute period after filling but before the initiation of photochemistry.

112   Particle-phase instrumentation sampled alternatingly every two minutes through a

113   thermodenuded or ambient sample line. The thermodenuder was operated at 300 ºC with a

114   residence time of approximately 5 s and volatilized semi-volatile components, including those that

115   are internally mixed with BC. The ambient line was lined with a charcoal cloth that removed excess

116   gases (such as VOCs, NO_x, and O_3) that could interfere with particle-phase measurements.

117   Comparison of thermodenuded versus ambient particles allowed for the investigation of coating

118   amount and volatility. The gas-phase composition in the mini chamber was similar to that sampled

119   directly from the fire (Koss et al., 2018;Lim et al., 2019). Particle phase instrumentation included:

120   a multi-wavelength cavity-ringdown-photoacoustic absorption spectrometer (CRD-PAS) and a

121   photoacoustic absorption spectrometer (PASS-3) for characterization of light absorption and

122   extinction coefficients at 405 nm, 532 nm, and 781 nm; a high resolution aerosol mass

spectrometer (HR-ToF-AMS) for characterization of non-refractory submicron particulate matter (NR-PM$_1$) components (i.e. OA, NO$_3$, SO$_4$, NH$_4$, Cl, K); a soot photometer AMS (SP-AMS) in laser-only mode for characterization of refractory BC and the NR-components that are internally mixed with BC; a single particle soot photometer (SP2) for characterization of refractory BC mass concentrations and size distributions; and a scanning electrical mobility sizer (SEMS) for measurement of particle mobility size distributions. Further details regarding instrument operation and calibration are provided in the Supplemental Material and in Lim et al. (2019).

3   Results and Discussion

3.1   Bulk optical property relationships

Due to the wide variety of biomass fuels and types used during FIREX, there was a substantial diversity in the properties of primary particles produced. Previous studies have shown both the single scatter albedo (SSA) and wavelength-dependence of absorption (the absorption Angstrom exponent, AAE) depend on the modified combustion efficiency (MCE) (Liu et al., 2013;McMeeking et al., 2014;Pokhrel et al., 2017). The MCE is defined here as:

$$MCE = \frac{[CO_2]}{[CO_2]+[CO]} \tag{1}$$

The SSA is defined as:

$$SSA = \frac{b_{ext}-b_{abs}}{b_{ext}} \tag{2}$$

where b_{ext} is the wavelength-specific extinction coefficient and b_{abs} is the wavelength-specific absorption coefficient. The AAE is defined as:

$$AAE = -\log(\frac{b_{abs,\lambda1}}{b_{abs,\lambda2}})/\log\left(\frac{\lambda1}{\lambda2}\right) \tag{3}$$

where λ_1 and λ_2 indicate two different wavelengths, here 405 nm and 532 nm. The MCE characterizes the overall combustion efficiency, with values closer to unity indicating more complete combustion. In general, higher MCE correspond to more flaming combustion conditions while smaller MCE correspond to more smoldering conditions. We find a similar relationship between SSA$_{405nm}$, AAE, and [OA]/[BC] with MCE as previous studies (**Figure 1**) (McMeeking

149   et al., 2009;Liu et al., 2013;McMeeking et al., 2014;Pokhrel et al., 2017). Specifically, the

150   SSA_{405nm} is relatively constant and near unity for MCE < ~0.9, but above this value exhibits a

151   rapid decline, albeit with a substantial amount of scatter (**Figure 1**a). The AAE is also relatively

152   constant when MCE < 0.9, with very large values (AAE ~ 8). There is a rapid, scattered decrease

153   in the AAE as MCE increases further (**Figure 1**b). The relationship between [OA]/[BC] and MCE

154   is similar, with values generally decreasing as MCE increases but a large amount of scatter (**Figure

155   1**d). There is also a general relationship between the mass absorption coefficient referenced to BC

156   (MAC_{BC}) at 405 nm and the MCE, but with similar scatter as the other properties (**Figure 1**c). The

157   MAC_{BC} is defined as:

158    $$MAC_{BC} = b_{abs}/[BC] \qquad\qquad\qquad\qquad (4)$$

159   The $MAC_{BC,405nm}$ includes contributions from absorption by BC, BrC, and from coating-induced

160   enhancement of BC absorption. These results, along with the literature, indicate that MCE can

161   provide guidance as to the general magnitude of these particle properties, but that the MCE is

162   ultimately a fairly imprecise metric, especially for the SSA_{405nm}.

163   However, we find a very strong relationship between the SSA_{405nm} and the total [OA]/[BC]

164   ratio (**Figure 1**e). This is consistent with the findings of Pokhrel et al. (2016), who observed

165   something similar but over a smaller range of [OA]/[BC]. (Similarly strong relationships are

166   observed for SSA values at 532 nm and 781 nm (**Figure S1**), or if the [NR-PM$_1$]/[BC] are used as

167   OA averages 95% of the total NR-PM$_1$ mass.) Smaller [OA]/[BC] correspond to smaller SSA_{405nm}

168   values with a sigmoidal relationship observed. (Fit parameters for all fits shown are provided in

169   **Table S1**.) There is similarly a very strong, sigmoidal relationship between the AAE and

170    $MAC_{BC,405nm}$ and [OA]/[BC] (**Figure 1**f,g). The large increase in the $MAC_{BC,405nm}$ indicates that

171   BrC contributes substantially to the total absorption. The contributions of coating-induced

172   enhancements and of BrC are discussed further in Sections 3.4.1 and 3.4.2. The larger range of

173   [OA]/[BC] and the greater number of individual burns considered here, compared to Pokhrel et al.

174   (2016), allows for determination of more robust fits. Pokhrel et al. (2017) found that the absorption

175   enhancement at 405 nm, determined from thermodenuder measurements, increased with

176   [OA]/[BC] up to [OA]/[BC] ~33 (the largest value reported), consistent with our findings.

177   These observations demonstrate that the optical properties of the primary particles depend on the

178   relative amount of OA versus BC. This is as expected because OA is generally more scattering,

179 compared to BC, and light absorbing OA (aka BrC) typically exhibits a much stronger wavelength

180 dependence than BC. Based on these relationships, we divide the individual burns into different

181 classes (**Table 1**). We have chosen to classify particles based on the observed SSA_{405nm} values;

182 use of [OA]/[BC] for classification yields largely similar results, given the strong relationship

183 between the two. The dividing lines between classes are selected to yield six classes that span the

184 entire range of SSA_{405nm} values, from 0.23 (Class 1) to 0.97 (Class 6), with approximately equal

185 numbers of individual burns in each class (ca. 8-10). Partitioning the observations into different

186 particle classes facilitates interpretation of the photochemical evolution of the particles, to be

187 discussed in future work. In addition, we find that use of the Class average properties versus MCE

188 generally provides more representative fits to the observations (visually apparent in **Figure 1**, and

189 supported by the reduced χ^2 for the fits).

3.2   OA composition and volatility

191 Variability in the bulk composition of the OA is characterized by the O:C and H:C atomic

192 ratios and the fractional abundance (f_x) of two marker ions, $m/z = 44$ and $m/z = 60$. The f_{44} is

193 complementary to O:C and larger values generally indicate a greater degree of oxygenation and

194 the presence of carboxylic acids. The f_{60} is often taken as a marker ion for biomass burning, in

195 particular a signature of levoglucosan and similar molecules (Schneider et al., 2006;Alfarra et al.,

196 2007). The high resolution ion $C_2H_4O_2^+$ contributes to and exhibits similar behavior as f_{60}; the

197 slope for $f_{C2H4O2+}$ against f_{60} is 0.98. While it is known that properties such as f_{60} vary in different

198 biomass burning samples (Schneider et al., 2006) or between near-source intercepts of different

199 ambient plumes (Garofalo et al., 2019), the specific dependence on burn conditions or overall

200 particle composition (e.g. [OA]/[BC]) has not been systematically explored to our knowledge.

201 The average $f_{60} = 0.022 \pm 0.01$ (1σ). The f_{60} values vary non-monotonically with [OA]/[BC],

202 exhibiting a slight increase from Class 1 to Class 3 and then a decrease from Class 4 to Class 6

203 (Figure 2a). This indicates that, while f_{60} is overall a useful marker ion for biomass burning, it

204 cannot be used to distinguish between different burn conditions. The f_{44} generally decreases with

205 [OA]/[BC] (Figure 2b; $r^2 = 0.33$.) However, the average f_{44} values for particle Classes 2-5 differ

206 negligibly, suggesting that f_{44} might be useful in discriminating between extreme cases (e.g. Class

207 1 versus Class 6), but that it is of limited general use in distinguishing between burn conditions

208 and fuel types. The O:C atomic ratio (average $= 0.37 \pm 0.09$) exhibits similar behavior—expected

209   as f_{44} is generally related to O:C (Aiken et al., 2008)—with a general decrease as [OA]/[BC]

210   increases, although a comparably weaker correlation (Figure 2c; $r^2 = 0.17$). The H:C (average =

211   1.76 ± 0.05) exhibits a weak, positive correlation with [OA]/[BC], although the variability is slight

212   (Figure 2d; $r^2 = 0.27$).

213   The mass fraction of the OA that is composed of nitrated organics ($f_{ON\text{-}OA}$ = [ON]/[OA]) was

214   determined using the HR-ToF-AMS measurements and the method of Kiendler-Scharr et al.

215   (2016) (see the Supplemental Material for further details). The terminology nitrated organics (ON)

216   includes contributions from both nitro and nitrate functional groups. The fraction of measured

217   nitrate that was ON ($f_{ON\text{-}N}$ = [ON]/([ON]+[NO$_3^-$])) decreased with [OA]/[BC] and ranged from 0.91

218   (Class 1) to 0.48 (Class 6) (**Figure S2a**). The Class-specific average $f_{ON\text{-}OA}$ also decreased with

219   [OA]/[BC], although by a much greater extent than the $f_{ON\text{-}N}$, ranging from 6.0% (Class 1) to 0.27%

220   (Class 6) and (**Figure 2e**). There is a reasonably linear relationship between log($f_{ON\text{-}OA}$) and

221   log([OA]/[BC]) (r^2 = 0.47). This indicates that a larger proportion of ON species and

222   functionalities are produced when particles are, on average, more BC-rich. This does not reflect

223   differences in fuel nitrogen content as there is no relationship between fuel N and $f_{ON\text{-}OA}$ (**Figure**

224   **S2b**). Therefore, it seems that the relationship between $f_{ON\text{-}OA}$ and [OA]/[BC] is related more so to

225   the burn conditions than the fuel N content, although as with many other properties the relationship

226   with [OA]/[BC] is clearer than with the MCE (**Figure S2c**).

227   The OA volatility is characterized as the ratio between the OA concentration after

228   thermodenuding to that without thermodenuding (the mass fraction remaining, MFR$_{OA}$). The

229   MFR$_{OA}$ decreases as [OA]/[BC] increases (**Figure 2f**), indicating that the OA at lower [OA]/[BC]

230   is less volatile than the OA at higher values. This observation provides support for the proposal by

231   Saleh et al. (2014) that less volatile, more absorbing species are preferentially formed under

232   conditions where BC formation is favored, discussed further in Section 3.4.2. The relationship

233   between MFR$_{OA}$ and [OA]/[BC] is reasonably described by an exponential function.

3.3   BC Mixing State

235   As discussed above, the relative amounts of OA and BC vary greatly between fuel types and

236   combustion conditions. However, the distribution of BC and OA between particles, and how this

237   varies between very different burn conditions, has not been previously explored in detail to our

knowledge. The bulk average fraction of OA that is internally mixed with BC versus OA that is externally mixed from BC is determined using the HR-ToF-AMS and SP-AMS measurements. The HR-ToF-AMS quantifies OA independent of mixing state, whereas the SP-AMS (as operated here) quantifies only the OA that is internally mixed with BC. The fraction of OA that is internally mixed with BC ($f_{OA,int}$) is:

$$f_{OA,int} = \frac{[OA]_{SP-AMS}}{[OA]_{HR-ToF-AMS}} = \frac{[OA]_{int}}{[OA]_{tot}} \tag{5}$$

where the subscript *int* indicates the OA that is internally mixed with BC and the subscript *tot* indicates the total OA. The $f_{OA,int}$ should range from 0 to 1. Related, the SP-AMS quantified the ratio between the OA that is internally mixed with BC and the BC concentration, referred to here as $[OA]_{int}/[BC]$. We find that $f_{OA,int}$ decreases substantially as $[OA]/[BC]$ increases, ranging from $f_{OA,int} = 0.4$ for Class 1 (low SSA) particles to $f_{OA,int} = 0.01$ for Class 6 (high SSA) particles (**Figure 3a**). The data are well-fit by a sigmoidal function. However, the amount of OA coating BC ($R_{OA-BC} = [OA]_{int}/[BC]$) increases with the total $[OA]/[BC]$, also with a sigmoidal relationship (**Figure 3b**). Thus, while a smaller fraction of the total OA is internally mixed with BC for larger total $[OA]/[BC]$ the amount of OA that coats BC increases. Most likely this behavior reflects that BC and OA are generated with different efficiencies in different parts of the combusting biomass. BC is more efficiently generated from flaming combustion while OA is more efficiently generated from smoldering combustion. These observations demonstrate that the extent to which atmospheric models can assume that all OA is internally mixed with or externally mixed from BC at the point of emission will depend on the combustion conditions.

3.4 Absorption enhancement and brown carbon

3.4.1 Coating-induced absorption enhancement

Non- or weakly-absorbing coatings on black carbon particles can theoretically increase the absorption by BC (Fuller et al., 1999;Bond et al., 2006), an effect which has been confirmed by laboratory experiments (Lack et al., 2009;Shiraiwa et al., 2010;Cappa et al., 2012). The extent to which coatings on BC actually enhance absorption by BC in the atmosphere remains unclear. Some studies indicate minor coating-induced enhancements while others indicate substantial enhancements (Cappa et al., 2012;Healy et al., 2015;Liu et al., 2015;Peng et al., 2016;Zhang et al.,

266 2016;Liu et al., 2017;Cappa et al., 2019b). Understanding the nature of the coating-induced

267 enhancement is important for quantifying the radiative impacts of BC (Jacobson, 2001;Bond et al.,

268 2013). Further, these coating-induced absorption enhancements ($E_{abs.coat}$) complicate the

269 determination of brown carbon (BrC) absorption and the two must be separated. Here, we examine

270 the extent to which coatings on BC for primary biomass burning particles enhance the BC

271 absorption. Theoretically, the magnitude of $E_{abs,coat}$ for an individual particle depends primarily on

272 the coating thickness and secondarily on the size of the BC core (Bond et al., 2006; Fuller et al.,

273 1999). Thus, the extent to which coatings enhance BC absorption for a given situation can be

274 assessed through the relationship between the observed MAC_{BC} and the coating-to-core mass ratio

275 ($R_{coat-rBC} = [NR-PM]_{int}/[BC]$, where int indicates that the coating material is internally mixed with

276 BC). The expectation is that the MAC_{BC} increases with $R_{coat-BC}$.

277   However, absorption by BrC can also lead to an apparent increase in the normalized absorption

278 with R_{BC} if the BrC abundance correlates with the total coating amount. Because BrC absorbs more

279 strongly at shorter wavelengths, the wavelength-dependence of the MAC_{BC} to R_{BC} relationship can

280 be used to further separate the influence of coating versus BrC absorption. The MAC_{BC} exhibits a

281 wavelength-dependent relationship with $R_{coat-rBC}$ for fresh biomass particles (405 nm, 532 nm and

282 781 nm) (**Figure 4a-c**). The MAC_{BC} increases notably with $R_{coat-rBC}$ at 405 nm and to a lesser extent

283 at 532 nm. At 781 nm the MAC_{BC} is essentially independent of $R_{coat-rBC}$ up to $R_{coat-rBC}$ values as

284 large as 10, but does exhibit some increase at $R_{coat-rBC} > 10$. However, this is most likely a result

285 of absorption by OA at 781 nm and not indicative of an increase in the coating-induced

286 enhancement, discussed further below. The wavelength dependence provides clear evidence of

287 BrC absorption at shorter wavelengths.

288   That the MAC_{BC} at 781 nm is nearly independent of $R_{coat-rBC}$ up to such large $R_{coat-rBC}$ values

289 indicates that there is only a minor coating-induced enhancement for the primary biomass particles,

290 the magnitude of which is discussed below. Our observations are consistent with McMeeking et

291 al. (2014), who also investigated the relationship between the MAC_{BC} and $R_{coat-rBC}$ for a primary

292 biomass particles from multiple fuel types. Most likely, this lack of a substantial coating-induced

293 enhancement results from a non-even distribution of non-BC mass across the population of BC

294 particles (Fierce et al., 2016;Liu et al., 2017) and from the morphology of BC-containing particles

295 not conforming to an idealized core-shell structure (Adachi et al., 2010). The influence of

296 photochemical aging on the coating-induced enhancement will be examined in future work.

297   The relationship between MAC_{BC} and the coating amount ($R_{coat\text{-}rBC}$) can be contrasted with the

298   relationship between MAC_{BC} and the total [OA]/[BC]. At all three wavelengths the MAC_{BC} exhibit

299   strong, sigmoidal relationships with [OA]/[BC] (**Figure 4d-f**). That $MAC_{BC,781nm}$ exhibits such a

300   clear relationship with [OA]/[BC] suggests that even the small apparent coating-induced

301   enhancement, implied above from the very weak with $R_{coat\text{-}rBC}$, is largely driven by absorption by

302   BrC rather than from the impact of coating on BC. Pokhrel et al. (2017) found that the absorption

303   enhancement, determined from thermodenuder measurements, increased notably with [OA]/[BC]

304   up to [OA]/[BC] ~33 at 405 nm (the largest value reported by them), but by much less at 660 nm,

305   consistent with our findings.

306   The observations allow for determination of wavelength-dependent MAC_{BC} values for pure BC

307   ($MAC_{BC,pure}$) for each wavelength by extrapolation of the MAC_{BC} versus [OA]/[BC] ratio to zero

308   using sigmoid fits. Since the $R_{coat\text{-}rBC}$ correlates reasonably with [OA]/[BC] (**Figure 3**b),

309   extrapolation against [OA]/[BC] to zero effectively removes both contributions from BrC and any

310   coating-induced enhancement. The derived $MAC_{BC,pure}$ values are 11.8 m^2 g^{-1} at 405 nm, 8.8 m^2

311   g^{-1} at 532 nm and 5.5 m^2 g^{-1} at 781 nm, with estimated fit-based uncertainties of ~10%. The

312   absolute uncertainties on the $MAC_{BC,pure}$ are primarily dependent on the uncertainty in the b_{abs} and

313   [rBC] measurements, and are ~35%. The derived MAC_{BC} values are very similar to those recently

314   reported by Forestieri et al. (2018) for fresh BC particles: $MAC_{BC,pure}$ = 11.9 m^2 g^{-1} at 405 nm and

315   8.8 m^2 g^{-1} at 532 nm, with an extrapolated value at 781 nm of 5.7 m^2 g^{-1}. The value at 532 nm is

316   somewhat higher than that suggested by Bond and Bergstrom (2006) (7.75 m^2 g^{-1} at 532 nm). Our

317   derived $MAC_{BC,pure}$ values yield an AAE = 1.17, determined from a fit to the three wavelengths. An

318   AAE close to unity indicates absorption is dominated by BC, as expected.

319   Values for the absorption enhancement at 781 nm are calculated as the ratio between the

320   observed MAC_{BC} in **Figure 4** and the derived $MAC_{BC,pure}$. The derived E_{abs} range from 0.96 to 27.

321   Values greater than two occur only for the particles having particularly large [OA]/[BC], > 400.

322   As E_{abs} values much greater than two at 781 nm are unlikely to result from mixing-induced

323   enhancements (Chakrabarty and Heinson, 2018), this again suggests that the OA is somewhat

324   absorbing at this wavelength. For the burns where [OA]/[BC] < 400, the median E_{abs} = 1.14 and

325   the arithmetic mean E_{abs} = 1.19 ± 0.14 (1σ). Given that some of this enhancement may result from

326   BrC absorption at 781, these values can be considered upper-limits on $E_{abs,coat}$, and the small

327 magnitude is consistent with our conclusion above that, while likely greater than zero, the mixing-
328 induced enhancement is generally negligible. It is possible that the $E_{abs,coat}$ values when [OA]/[BC]
329 > 400 are substantially larger. However, given the general lack of a dependence of the $MAC_{BC,781nm}$
330 for $R_{BC\text{-}coat}$ < 10 this seems unlikely.

331 ### 3.4.2 Primary brown carbon absorption

332 The absorption due to brown carbon is determined by difference as:

333 $$b_{abs,BrC} = b_{abs,obs} - MAC_{BC,pure} \cdot [BC] \cdot E_{abs,coat} \qquad (6)$$

334 where $b_{abs,BrC}$ is the absorption due to BrC specifically. Importantly, the use of study-specific
335 $MAC_{BC,pure}$ values serves to reduce systematic biases in the $b_{abs,BrC}$, compared to direct use of
336 literature $MAC_{BC,pure}$ values. Assuming $E_{abs,coat} = 1$ provides an upper limit on the BrC absorption,
337 which we note is likely most appropriate for the particles sampled here, as discussed in the previous
338 section. Therefore, we use the upper-limit values throughout the analysis that follows, unless
339 otherwise stated. However, a lower limit for BrC absorption can be determined at 405 nm and 532
340 nm assuming that all of the enhancement at 781 nm results from coatings and not from BrC. The
341 resulting $E_{abs,obs}$ ($= MAC_{BC,obs}/MAC_{BC,pure}$) at 781 nm averages 1.19 for $R_{BC\text{-}coat}$ < 10. Using $E_{abs,coat}$
342 = 1.19 in Eqn. 7 yields a lower limit for the BrC absorption at the two shorter wavelengths,
343 appropriate since $E_{abs,coat}$ generally has only a small wavelength dependence. A fit to the coating-
344 corrected (lower-limit) versus upper-limit $b_{abs,BrC}$ yields a slope of 0.97 at 405 nm and 0.88 at 532
345 nm (**Figure S3**). The smaller difference at 405 nm results from the fractional contribution of BrC
346 to the total absorption being larger at this wavelength.

347 Brown carbon-specific mass absorption coefficients (MAC_{BrC}) are determined as the ratio
348 between $b_{abs,BrC}$ and the total OA concentration:

349 $$MAC_{BrC} = \frac{b_{abs,BrC}}{[OA]} \qquad (7)$$

350 The MAC_{BrC} values from Eqn. **7** are bulk-average values, and do not account for different
351 molecules and classes of molecules likely having different absorptivities. Uncertainties in the
352 MAC_{BrC} values are determined by error propagation. Similarly, an AAE value for just the brown
353 carbon (AAE_{BrC}) can be calculated using wavelength pairs as:

$$AAE_{BrC} = -\log(\frac{b_{abs,BrC,\lambda_1}}{b_{abs,BrC,\lambda_2}})/\log\left(\frac{\lambda_1}{\lambda_2}\right);$$ (8)

The geometric averages of the MAC_{BrC} values are $0.76^{+0.65}_{-0.35}$ m^2 g^{-1}, $0.21^{+0.36}_{-0.13}$ m^2 g^{-1}, $0.056^{+0.15}_{-0.04}$ m^2 g^{-1} at 405 nm, 532 nm and 781 nm, with uncertainties the 1σ burn-to-burn variability. The MAC_{BrC} values vary between classes, generally increasing as the [OA]/[BC] ratio decreases at all wavelengths (shown for 405 nm in **Figure 5**a). For example, the average $MAC_{405nm} = 2.3 \pm 1$ m^2 g^{-1} for Class 1 and 0.35 ± 0.09 m^2 g^{-1} for Class 6. Although the uncertainties on the derived MAC_{BrC} increase substantially as [OA]/[BC] decreases—because BrC absorption contributes to a smaller extent at longer wavelengths—the observations nonetheless indicate that the BrC absorptivity depends on the combustion conditions. The relationship at 405 nm is well-described by a sigmoidal function in log-log space, with limiting values of 0.35 m^2 g^{-1} at large [OA]/[BC] and 11.2 m^2 g^{-1} at small [OA]/[BC]. That the extrapolated zero [OA]/[BC] limit for MAC_{BrC} is similar to pure BC suggests an evolution of BrC towards having properties similar to BC when the overall [OA] content is small. Such behavior is consistent with Saleh et al. (2018), who argue that there is a continuum of BrC properties that depends on the combustion conditions, as demonstrated in that study for low-temperature benzene and toluene combustion. The range of the MAC_{BrC} values observed here, including that there is notable absorption at 781 nm, encompass many previous measurements, summarized in **Table S3**. This likely reflects the wide diversity of fuel types and burn conditions considered here, as exemplified by the very large range of [OA]/[BC].

Estimated values of the imaginary component of the refractive index for BrC (k_{BrC}) are determined from Mie theory via optical closure (Zhang et al., 2016), assuming a real part of the refractive index of 1.5 and a particle diameter of 150 nm, a typical value for these experiments. Imaginary RI values are of use in atmospheric models for calculation of BrC absorption. There is a linear relationship between MAC_{BrC} and k_{BrC} (**Figure S4**a). Thus, the k_{BrC} exhibits a similar correlation with [OA]/[BC] as does the MAC_{BrC} (**Figure 5**a).

The wavelength-dependence of absorption, i.e. the $AAE_{405-532}$, also varies with [OA]/[BC], in this case with a positive relationship between the two (**Figure 5**b). The relationship is reasonably described by a sigmoidal function. This implies that, while the MAC_{BrC} varies inversely with [OA]/[BC] at all wavelengths, the exact variation is wavelength dependent. The $AAE_{405-532}$ relationship with [OA]/[BC] is well-described by a sigmoidal function (versus log([OA]/[BC]),

383   with limiting values of 10.4 at large [OA]/[BC] and 1.3 at small [OA]/[BC]. The wavelength-

384   dependence of the k_{BrC} (w_{BrC}) are also calculated, to facilitate comparison with the literature, as:

385    $$w_{BrC} = -\log\left(\frac{k_{BrC,\lambda 1}}{k_{BrC,\lambda 2}}\right)/\log(\frac{\lambda 1}{\lambda 2})$$ (9)

386   The w_{BrC} exhibit a similar dependence on [OA]/[BC] as the AAE_{BrC}, as the w_{BrC} and AAE_{BrC} are

387   linearly related, albeit with some scatter (**Figure S4**b; $r^2 = 0.97$).

388   Our observations support the results of Saleh et al. (2014), who also found a relationship between

389   the $k_{BrC,405nm}$ and [OA]/[BC]. However, our analysis substantially extends the range of [OA]/[BC]

390   values investigated in that work (they considered [OA]/[BC] from only ca. 2 to 170). In the overlap

391   region between our two studies the $k_{BrC,405nm}$ agree reasonably well over the range 2 < [OA]/[BC]

392   < 50, but the $k_{BrC,405nm}$ from Saleh et al. (2014) are smaller than observed here above [OA]/[BC] =

393   50. Importantly, our results demonstrate that the linear fit suggested by Saleh et al. (2014) for

394   MAC_{BrC} is only appropriate over the range of values they considered and that a sigmoidal provides

395   for a more robust relationship over a wider range of [OA]/[BC]. Related, the wider range of

396   [OA]/[BC] enables more robust determination of the functional dependence of the wavelength-

397   dependence of absorption (w_{BrC}), with overall larger w_{BrC} values and a larger plateau at high

398   [OA]/[BC] compared to the fit by Saleh et al. (2014).

399   The MAC_{BrC} values also correlate with the nitrated organic fraction of OA, the latter of which, as

400   noted above, also correlates with the [OA]/[BC] (**Figure 6**a). This observation suggests that

401   organic nitrate and nitro functionalities may be at least somewhat responsible for the increase in

402   absorption. Laskin et al. (2018) performed offline molecular level analyses of primary OA

403   collected during FIREX. They found that nitroaromatics and N-containing polycyclic aromatic

404   hydrocarbons (PAHs) contribute notably to the total light absorption by BrC, although there are

405   many non-N-containing species that also contribute to BrC absorption. The variability between

406   particle Classes is consistent with the results of Lin et al. (2016), which show that the abundance

407   of N-containing chromophores varies between particles produced from different biomass fuels.

408   Additionally Mohr et al. (2013) observed a relationship between the concentration of nitrated

409   phenols and short-wavelength absorption by BrC, although it is possible that for their

410   measurements these species were produced from chemical processing, as opposed to being directly

411   emitted. Altogether, our results provide support for the idea that nitrated organic functionalities

412 are an important contributor to BrC absorption. However, it is very likely that other functional

413 groups also contribute to the total absorption.

414 The $MAC_{BrC,405nm}$ exhibits an inverse correlation with the f_{60}/f_{44} ratio of the OA, although there is

415 substantial scatter in the f_{60}/f_{44} ratio for a given particle class (**Figure 6**b). (The f_{44} and f_{60} have no

416 discernable relationship.) The observed $MAC_{BrC,405nm}$ relationship with f_{60}/f_{44} is opposite that

417 reported by Lack et al. (2013) for ambient measurements of particles a biomass burning plume,

418 who find a reasonable positive correlation. This difference in behavior results from our sampling

419 primary particles directly—thereby focusing on the inherent variability in the properties of the

420 emitted particles—while Lack et al. (2013) sampled ambient particles. For ambient sampling, the

421 observed relationship will be sensitive to mixing of biomass burning particles with background or

422 aged biomass particles, which are known to have a smaller f_{60} (Cubison et al., 2011). Thus, the

423 relationship observed by Lack et al. (2013) can best be viewed as a mixing line between the fresh

424 primary particles (having large $MAC_{BrC,405nm}$ and large f_{60}/f_{44}) and background or aged biomass

425 particles (having small $MAC_{BrC,405nm}$ and small f_{60}/f_{44}), rather than providing information on the

426 inherent variability in the absorptivity of the fresh particles.

427 ### 3.5   Size distributions

428   Total particle mobility size distributions and BC-only size distributions were measured (**Figure**

429 **7**). Primary particle size distributions are important parameters specified in regional and global

430 models. The number-weighted and volume-weighted size distributionare generally described by

431 either one or two log-normal modes for individual burns; a two-mode fit provides a more robust

432 solution across all modes. The mass-weighted BC size distributions are similarly described by one

433 or two log-normal modes. A fit to the average number-weighted distribution across all particle

434 classes yields geometric median diameters ($d_{p,N}$) and widths (σ_g) of 60.3 nm and 1.76, respectively,

435 for the smaller mode and 153 nm and 1.64 for the larger mode (**Figure 8**). The amplitude of the

436 smaller mode is 4.6 times the larger mode. A single mode fit yields $d_{p,N}$ = 68 nm and χ_g = 1.93,

437 although the fit is poorer. Mann et al. (2014) report $d_{p,N}$ values used by a variety of global models

438 for biofuels. The models tend to use either 80 nm or 150 nm, although a few use other values (30

439 nm, 60 nm, 100 nm). Those using 80 nm typically use σ_g = 1.80 while those using 150 nm typically

440 use σ_g = 1.59, although there are exceptions. Our observations indicate that use of a bimodal

441   distribution within models would be more representative, but that a single mode can do acceptably.

442   We find that the volume-weighted distribution calculated from a single-mode fit to the number-

443   weighted distribution is similar to the observed volume-weighted distribution (**Figure 8**). Thus,

444   the use of a single-mode to represent biomass burning size distributions thus appears acceptable,

445   so long as the appropriate parameters are used. In this context, the widths of the distribution used

446   by the various global models appear somewhat too small. However, we note that the microphysics

447   occurring in the fresh smoke sampled here, which will govern the size distributions, may differ

448   from that in atmospheric plumes.

449   The average BC-specific mass-weighted size distribution mode is at 148 nm (**Figure 8**). A

450   bimodal fit yields values for the mass median diameter ($d_{p,M}$) and σ_g of 137.2 nm and 1.62,

451   respectively, for the smaller mode and 197.1 nm and 1.24 for the larger mode, with most of the

452   mass contained in the smaller mode. May et al. (2014) report $d_{p,M}$ from laboratory biomass

453   combustion ranging from 140-190 nm, averaging 170 nm. Their average is somewhat larger than

454   ours, likely reflecting differences in the exact fuels sampled. The mode diameter for the BC-

455   specific distribution is especially smaller than observed for biomass burning particles from some

456   ambient observations, which tend to give values closer to 200 nm (Schwarz et al., 2008;Kondo et

457   al., 2011;Sahu et al., 2012;May et al., 2014;Cappa et al., 2019b). This difference between lab and

458   field observations was also noted by May et al. (2014). We speculate that the influence of

459   coagulation may be suppressed in our experiments relative to what occurs in the atmosphere due

460   to slower overall dilution, leading to smaller BC size distributions. To the extent this is the reason

461   for the difference, the total particle distributions would also be biased towards too small particles,

462   compared to the atmosphere. However, there is no relationship between $d_{p,N}$ and the total particle

463   number concentration for our experiments. Formation of secondary aerosol in the near-field of a

464   sampled ambient plume could also contribute to this difference.

465   There is substantial variability between individual burns within a given particle Class in terms

466   of the shape of the size distributions (**Figure 7**). This variability is most evident for Class 1, 2 and

467   5, but present for all Classes. Nonetheless, the number-weighted mean diameter ($d_{p,N,mean}$) appears

468   to decrease somewhat with MCE (**Figure 9**; $r^2 = 0.38$). However, the relationship is largely driven

469   by the Class 6 particles, which generally have lower MCE values, having larger $d_{p,N,mean}$ values. A

470   lack of any particularly clear relationship is consistent with Hosseini et al. (2010), who observed

471   the $d_{p,N,mean}$ to exhibit a complex relationship with combustion conditions. The $d_{p,N,mean}$ varies non-

472   monotonically with [OA]/[BC], with particle size first decreasing slightly as [OA]/[BC] increases

473   (from Class 1 to Class 3) and then increasing with further increases in [OA]/[BC] (from Class 4 to

474   Class 6) (**Figure 9**). This is despite the notable burn-to-burn variability. It is important to note that

475   the mobility-based size is particle shape-dependent; very BC-rich particles are more likely to have

476   non-spherical shapes and thus have larger mobility diameters. This could explain the minimum in

477     $d_{p,N}$ around Class 3 particles, for which [OA]/[BC] = 10.

478   Some of the variability within a class appears related to the presence of different fuel types

479   within a class. Number-weighted and BC-specific mass-weighted size distributions by fuel type

480   are shown in **Figure 10**. For the number-weighted distributions, leaf litter and rotten logs exhibit

481   the greatest variability between different burns, although we note that multiple burns were not

482   performed for all fuels. The shapes of the leaf litter, peat and "other" fuel types differ most notably

483   from the other fuel types, with the presence of more than one mode more apparent. (The "other"

484   category here includes non-traditional biofuels, specifically building materials and excelsior.) For

485   the BC-specific size distributions, the litter, canopy, and duff exhibited the greatest intra-fuel

486   variability. For most fuels, the BC-specific distribution peaks around 150 nm, as noted above.

487   However, for a subset of burns (eight of them) the BC-specific distribution peaks around 100 nm

488   (**Figure 10**). These small BC-mode distributions occur for the OA-rich particle classes 4, 5 and 6

489   (**Figure 7**), although there is no clear pattern to their occurrence.

490   **4   Conclusions and Implications**

491   Measurements of primary particles produced from combustion of a variety of biomass fuel

492   types indicate the optical, physical, and chemical properties of the emitted particles exhibit wide

493   variability. We show that variability in many optical properties (e.g. single scatter albedo,

494   wavelength dependence of absorption, mass absorptivity of black and brown carbon) is directly

495   linked to the [OA]/[BC] ratio of the emitted particles; the relationships with [OA]/[BC] are much

496   stronger than with the commonly used modified combustion efficiency, and mathematical

497   relationships between the various properties are determined. However, the absorption

498   enhancement due to coating of BC (the so-called "lensing" effect) is shown to be negligible and

499   essentially independent of the amount of coating up to large coating-to-BC mass ratios. The brown

500   carbon mass absorptivity correlates with the nitrated organic fraction of OA, suggesting that

nitrated organic species contribute to BrC absorption. Many bulk chemical properties (i.e. O:C, H:C, and the relative concentrations of key marker ions such as f_{60}) exhibit limited dependence on the burn conditions and the [OA]/[BC] ratio. However, both the OA volatility and nitrated organic fraction of OA decrease with [OA]/[BC]. The fraction of OA that is internally mixed with BC was shown to decrease strongly with the [OA]/[BC] ratio, from nearly all OA being internally mixed with BC when the particles are overall BC-rich to only a few percent of OA being mixed with BC when OA dominates. Yet, the relative amount of OA coating the BC increases with [OA]/[BC]; that is, when more of the OA is externally mixed from BC those particles that do contain BC nonetheless have thicker OA coatings. The observed total particle size distributions are reasonably well described by a single log-normal mode, but are better fit using a bimodal distribution. The BC-specific size distributions are similarly best fit using a bimodal distribution, although a single mode provides a reasonable representation. The dependence of the geometric median mobility diameter on the burn conditions or particle state (i.e. the [OA]/[BC]) is complicated by the mobility diameter being sensitive to variations in particle shape, which depend on the [OA]/[BC] ratio. Overall, these results expand on previous observations of primary biomass burning particle properties, considering a wider range of [OA]/[BC] and associated properties. Further, they provide a foundation for understanding the post-emission evolution of biomass burning smoke due to photochemical oxidation as discussed in Lim et al. (2019).

5   Data Availability

All data are available from the NOAA FIREX-AQ data repository (https://esrl.noaa.gov/csd/projects/firex/firelab/). This includes a summary of the fuel types used for each burn and the measurement time-series for each burn. The primary particle averages used in this work are additionally collected in the UC DASH data repository (Cappa et al., 2019a).

6   Author Contributions

CDC and JHK designed the experiments. CDC, CYL, and DHH carried out the measurements and data processing. CDC, CDM, and CYL analyzed data. CDC and CDM wrote the manuscript, with contributions from all co-authors.

7 Acknowledgements

528

529   This work was supported by the National Oceanic and Atmospheric Administration
530   Atmospheric Chemistry, Carbon Cycle & Climate Program, awards NA16OAR4310111 and
531   NA16OAR4310112. CYL was additionally supported by the National Science Foundation
532   Graduate Research Fellowship Program. The entire FIREX team, especially Bob Yokelson and
533   Jim Roberts and the staff of the Missoula Fire Sciences Laboratory, are acknowledged for their
534   assistance. Putting together the community inlet was a community effort—thank you to all who
535   contributed. Shuka Schwarz and Gavin McMeeking are also thanked for their assistance with the
536   SP2.

8   References

Adachi, K., Chung, S. H., and Buseck, P. R.: Shapes of soot aerosol particles and implications for their effects on climate, J. Geophys. Res., 115, D15206, https://doi.org/10.1029/2009jd012868, 2010.

Adler, G., Flores, J. M., Abo Riziq, A., Borrmann, S., and Rudich, Y.: Chemical, physical, and optical evolution of biomass burning aerosols: a case study, Atmos. Chem. Phys., 11, 1491-1503, https://doi.org/10.5194/acp-11-1491-2011, 2011.

Aiken, A. C., Decarlo, P. F., Kroll, J. H., Worsnop, D. R., Huffman, J. A., Docherty, K. S., Ulbrich, I. M., Mohr, C., Kimmel, J. R., Sueper, D., Sun, Y., Zhang, Q., Trimborn, A., Northway, M., Ziemann, P. J., Canagaratna, M. R., Onasch, T. B., Alfarra, M. R., Prevot, A. S. H., Dommen, J., Duplissy, J., Metzger, A., Baltensperger, U., and Jimenez, J. L.: O/C and OM/OC ratios of primary, secondary, and ambient organic aerosols with high-resolution time-of-flight aerosol mass spectrometry, Environ. Sci. Technol., 42, 4478-4485, https://doi.org/10.1021/es703009q, 2008.

Alexander, D. T. L., Crozier, P. A., and Anderson, J. R.: Brown Carbon Spheres in East Asian Outflow and Their Optical Properties, Science, 321, 833-836, https://doi.org/10.1126/science.1155296, 2008.

Alfarra, M. R., Prevot, A. S. H., Szidat, S., Sandradewi, J., Weimer, S., Lanz, V. A., Schreiber, D., Mohr, M., and Baltensperger, U.: Identification of the Mass Spectral Signature of Organic Aerosols from Wood Burning Emissions, Environmental Science & Technology, 41, 5770-5777, https://doi.org/10.1021/es062289b, 2007.

Andreae, M. O., and Merlet, P.: Emission of trace gases and aerosols from biomass burning, Global Biogeochemical Cycles, 15, 955-966, https://doi.org/doi:10.1029/2000GB001382, 2001.

Bluvshtein, N., Lin, P., Flores, J. M., Segev, L., Mazar, Y., Tas, E., Snider, G., Weagle, C., Brown, S. S., Laskin, A., and Rudich, Y.: Broadband optical properties of biomass-burning aerosol and identification of brown carbon chromophores, Journal of Geophysical Research: Atmospheres, 122, 5441-5456, https://doi.org/doi:10.1002/2016JD026230, 2017.

Bond, T. C., and Bergstrom, R. W.: Light absorption by carbonaceous particles: An investigative review, Aerosol Science and Technology, 40, 27-67, https://doi.org/10.1080/02786820500421521, 2006.

Bond, T. C., Habib, G., and Bergstrom, R. W.: Limitations in the enhancement of visible light absorption due to mixing state, J. Geophys. Res.-Atmos., 111, https://doi.org/10.1029/2006JD007315, 2006.

Bond, T. C., Doherty, S. J., Fahey, D. W., Forster, P. M., Berntsen, T., DeAngelo, B. J., Flanner, M. G., Ghan, S., Kärcher, B., Koch, D., Kinne, S., Kondo, Y., Quinn, P. K., Sarofim, M. C., Schultz, M. G., Schulz, M., Venkataraman, C., Zhang, H., Zhang, S., Bellouin, N., Guttikunda, S. K., Hopke, P. K., Jacobson, M. Z., Kaiser, J. W., Klimont, Z., Lohmann, U., Schwarz, J. P., Shindell, D., Storelvmo, T., Warren, S. G., and Zender, C. S.: Bounding the role of black carbon in the climate system: A scientific assessment, Journal of Geophysical Research: Atmospheres, 118, 1-173, https://doi.org/10.1002/jgrd.50171, 2013.

Bruns, E. A., Perraud, V., Zelenyuk, A., Ezell, M. J., Johnson, S. N., Yu, Y., Imre, D., Finlayson-Pitts, B. J., and Alexander, M. L.: Comparison of FTIR and Particle Mass Spectrometry for the

Measurement of Particulate Organic Nitrates, Environmental Science & Technology, 44, 1056-1061, https://doi.org/10.1021/es9029864, 2010.

Canagaratna, M. R., Jayne, J. T., Jimenez, J. L., Allan, J. D., Alfarra, M. R., Zhang, Q., Onasch, T. B., Drewnick, F., Coe, H., Middlebrook, A., Delia, A., Williams, L. R., Trimborn, A. M., Northway, M. J., DeCarlo, P. F., Kolb, C. E., Davidovits, P., and Worsnop, D. R.: Chemical and microphysical characterization of ambient aerosols with the Aerodyne aerosol mass spectrometer, Mass Spectrometry Reviews, 26, 185-222, https://doi.org/10.1002/mas.20115, 2007.

Cappa, C. D., Onasch, T. B., Massoli, P., Worsnop, D., Bates, T. S., Cross, E., Davidovits, P., Hakala, J., Hayden, K., Jobson, B. T., Kolesar, K. R., Lack, D. A., Lerner, B., Li, S. M., Mellon, D., Nuaanman, I., Olfert, J., Petaja, T., Quinn, P. K., Song, C., Subramanian, R., Williams, E. J., and Zaveri, R. A.: Radiative absorption enhancements due to the mixing state of atmospheric black carbon, Science, 337, 1078-1081, https://doi.org/10.1126/science.1223447, 2012.

Cappa, C. D., Lim, C. Y., Hagan, D. H., and Kroll, J. H.: Measurements from the Fire Influence on Regional and Global Environments Experiment (FIREX) Fire Lab Mini Chamber Experiment, UC Davis DASH, Dataset, version 1, https://doi.org/10.25338/B8CK5N, 2019a.

Cappa, C. D., Zhang, X., Russell, L. M., Collier, S., Lee, A. K. Y., Chen, C.-L., Betha, R., Chen, S., Liu, J., Price, D. J., Sanchez, K. J., McMeeking, G., Williams, L. R., Onasch, T. B., Worsnop, D. R., Abbatt, J., and Zhang, Q.: Light absorption by ambient black and brown carbon and its dependence on black carbon coating state for two California, USA cities in winter and summer, Journal of Geophysical Research-Atmospheres, https://doi.org/10.1029/2018JD029501, 2019b.

Chakrabarty, R. K., Moosmüller, H., Chen, L. W. A., Lewis, K., Arnott, W. P., Mazzoleni, C., Dubey, M. K., Wold, C. E., Hao, W. M., and Kreidenweis, S. M.: Brown carbon in tar balls from smoldering biomass combustion, Atmospheric Chemistry and Physics, 10, 6363-6370, https://doi.org/10.5194/acp-10-6363-2010, 2010.

Chakrabarty, R. K., and Heinson, W. R.: Scaling Laws for Light Absorption Enhancement Due to Nonrefractory Coating of Atmospheric Black Carbon Aerosol, Physical Review Letters, 121, 218701, https://doi.org/10.1103/PhysRevLett.121.218701, 2018.

Chen, Y., and Bond, T. C.: Light absorption by organic carbon from wood combustion, Atmos. Chem. Phys., 10, 1773-1787, https://doi.org/10.5194/acp-10-1773-2010, 2010.

Coggon, M. M., Lim, C. Y., Koss, A. R., Sekimoto, K., Yuan, B., Cappa, C. D., Kroll, J. H., Selimovic, V., Zarzana, K. J., Brown, S. S., Roberts, J. M., Müller, M., Yokelson, R. J., Wisthaler, A., Krechmer, J., Jimenez, J. L., De Gouw, J., and Warneke, C.: OH-chemistry of volatile organic compounds emitted from laboratory and ambient biomass burning smoke: Influence of furans and oxygenated aromatics on ozone and secondary VOC formation., Atmos. Chem. Phys. Discuss., https://doi.org/10.5194/acp-2019-516, 2019.

Collier, S., Williams, L. R., Onasch, T. B., Cappa, C. D., Zhang, X., Russell, L. M., Chen, C.-L., Sanchez, K. J., Worsnop, D. R., and Zhang, Q.: Influence of emissions and aqueous processing on particles containing black carbon in a polluted urban environment: Insights from a soot particle – aerosol mass spectrometer, Journal of Geophysical Research-Atmospheres, *123*, 6648-6666, https://doi.org/10.1002/2017JD027851, 2018.

Cubison, M. J., Ortega, A. M., Hayes, P. L., Farmer, D. K., Day, D., Lechner, M. J., Brune, W. H., Apel, E., Diskin, G. S., Fisher, J. A., Fuelberg, H. E., Hecobian, A., Knapp, D. J., Mikoviny, T.,

Riemer, D., Sachse, G. W., Sessions, W., Weber, R. J., Weinheimer, A. J., Wisthaler, A., and Jimenez, J. L.: Effects of aging on organic aerosol from open biomass burning smoke in aircraft and laboratory studies, Atmos. Chem. Phys., 11, 12049-12064, https://doi.org/10.5194/acp-11-12049-2011, 2011.

Fierce, L., Bond, T. C., Bauer, S. E., Mena, F., and Riemer, N.: Black carbon absorption at the global scale is affected by particle-scale diversity in composition, Nat. Comm., 7, https://doi.org/10.1038/ncomms12361, 2016.

Forestieri, S. D., Helgestad, T. M., Lambe, A. T., Renbaum-Wolff, L. H., Lack, D. A., Massoli, P., Cross, E. S., Dubey, M. K., Mazzoleni, C., Olfert, J., Freedman, A., Davidovits, P., Onasch, T. B., and Cappa, C. D.: Measurement and modeling of the multi-wavelength optical properties of uncoated flame-generated soot, Atmos. Chem. Phys., 18, 12141-12159, https://doi.org/10.5194/acp-18-12141-2018, 2018.

Forrister, H., Liu, J., Scheuer, E., Dibb, J., Ziemba, L., Thornhill, K. L., Anderson, B., Diskin, G., Perring, A. E., Schwarz, J. P., Campuzano-Jost, P., Day, D. A., Palm, B. B., Jimenez, J. L., Nenes, A., and Weber, R. J.: Evolution of brown carbon in wildfire plumes, Geophysical Research Letters, 42, 4623-4630, https://doi.org/10.1002/2015GL063897, 2015.

Fuller, K. A., Malm, W. C., and Kreidenweis, S. M.: Effects of mixing on extinction by carbonaceous particles, J. Geophys. Res.-Atmos., 104, 15941-15954, https://doi.org/10.1029/1998jd100069, 1999.

Garofalo, L. A., Pothier, M. A., Levin, E. J. T., Campos, T., Kreidenweis, S. M., and Farmer, D. K.: Emission and Evolution of Submicron Organic Aerosol in Smoke from Wildfires in the Western United States, ACS Earth and Space Chem., 3, 1237-1247, https://doi.org/10.1021/acsearthspacechem.9b00125, 2019.

Healy, R., Wang, J., Jeong, C. H., Lee, A., Willis, M., Jaroudi, E., Zimmerman, N., Hilker, N., Murphy, M., and Eckhardt, S.: Light-absorbing properties of ambient black carbon and brown carbon from fossil fuel and biomass burning sources, Journal of Geophysical Research: Atmospheres, 120, 6619-6633, 2015.

Hoffer, A., Gelencser, A., Guyon, P., Kiss, G., Schmid, O., Frank, G. P., Artaxo, P., and Andreae, M. O.: Optical properties of humic-like substances (HULIS) in biomass-burning aerosols, Atmospheric Chemistry and Physics, 6, 3563-3570, 2006.

Hoffer, A., Tóth, A., Nyirő-Kósa, I., Pósfai, M., and Gelencsér, A.: Light absorption properties of laboratory-generated tar ball particles, Atmos. Chem. Phys., 16, 239-246, https://doi.org/10.5194/acp-16-239-2016, 2016.

Hosseini, S., Li, Q., Cocker, D., Weise, D., Miller, A., Shrivastava, M., Miller, J. W., Mahalingam, S., Princevac, M., and Jung, H.: Particle size distributions from laboratory-scale biomass fires using fast response instruments, Atmos. Chem. Phys., 10, 8065-8076, https://doi.org/10.5194/acp-10-8065-2010, 2010.

Jacobson, M. Z.: Strong radiative heating due to the mixing state of black carbon in atmospheric aerosols, Nature, 409, 695-697, https://doi.org/10.1038/35055518, 2001.

Jen, C. N., Hatch, L. E., Selimovic, V., Yokelson, R. J., Weber, R., Fernandez, A. E., Kreisberg, N. M., Barsanti, K. C., and Goldstein, A. H.: Speciated and total emission factors of particulate

organics from burning western U.S. wildland fuels and their dependence on combustion efficiency, Atmos. Chem. Phys., 19, 1013-1026, https://doi.org/10.5194/acp-19-1013-2019, 2019.

Kiendler-Scharr, A., Mensah, A. A., Friese, E., Topping, D., Nemitz, E., Prevot, A. S. H., Äijälä, M., Allan, J., Canonaco, F., Canagaratna, M., Carbone, S., Crippa, M., Dall Osto, M., Day, D. A., De Carlo, P., Di Marco, C. F., Elbern, H., Eriksson, A., Freney, E., Hao, L., Herrmann, H., Hildebrandt, L., Hillamo, R., Jimenez, J. L., Laaksonen, A., McFiggans, G., Mohr, C., O'Dowd, C., Otjes, R., Ovadnevaite, J., Pandis, S. N., Poulain, L., Schlag, P., Sellegri, K., Swietlicki, E., Tiitta, P., Vermeulen, A., Wahner, A., Worsnop, D., and Wu, H.-C.: Ubiquity of organic nitrates from nighttime chemistry in the European submicron aerosol, Geophysical Research Letters, 43, 7735-7744, https://doi.org/doi:10.1002/2016GL069239, 2016.

Kirchstetter, T. W., Novakov, T., and Hobbs, P. V.: Evidence that the spectral dependence of light absorption by aerosols is affected by organic carbon, Journal of Geophysical Research-Atmospheres, 109, D21208, 2004.

Kondo, Y., Matsui, H., Moteki, N., Sahu, L., Takegawa, N., Kajino, M., Zhao, Y., Cubison, M. J., Jimenez, J. L., Vay, S., Diskin, G. S., Anderson, B., Wisthaler, A., Mikoviny, T., Fuelberg, H. E., Blake, D. R., Huey, G., Weinheimer, A. J., Knapp, D. J., and Brune, W. H.: Emissions of black carbon, organic, and inorganic aerosols from biomass burning in North America and Asia in 2008, J. Geophys. Res., 116, D08204, https://doi.org/10.1029/2010jd015152, 2011.

Koss, A. R., Sekimoto, K., Gilman, J. B., Selimovic, V., Coggon, M. M., Zarzana, K. J., Yuan, B., Lerner, B. M., Brown, S. S., Jimenez, J. L., Krechmer, J., Roberts, J. M., Warneke, C., Yokelson, R. J., and de Gouw, J.: Non-methane organic gas emissions from biomass burning: identification, quantification, and emission factors from PTR-ToF during the FIREX 2016 laboratory experiment, Atmos. Chem. Phys., 18, 3299-3319, https://doi.org/10.5194/acp-18-3299-2018, 2018.

Lack, D. A., Cappa, C. D., Cross, E. S., Massoli, P., Ahern, A. T., Davidovits, P., and Onasch, T. B.: Absorption Enhancement of Coated Absorbing Aerosols: Validation of the Photo-Acoustic Technique for Measuring the Enhancement, Aerosol Science and Technology, 43, 1006-1012, https://doi.org/10.1080/02786820903117932, 2009.

Lack, D. A., Langridge, J., Bahreni, R., Cappa, C. D., Middlebrook, A., and Schwarz, J. P.: Brown Carbon and Internal Mixing in Biomass Burning Particles, PNAS, 10, 14802-14807, https://doi.org/10.1073/pnas.1206575109, 2012a.

Lack, D. A., Richardson, M. S., Law, D., Langridge, J. M., Cappa, C. D., McLaughlin, R. J., and Murphy, D. M.: Aircraft Instrument for Comprehensive Characterization of Aerosol Optical Properties, Part 2: Black and Brown Carbon Absorption and Absorption Enhancement Measured with Photo Acoustic Spectroscopy, Aerosol Science and Technology, 46, 555-568, https://doi.org/10.1080/02786826.2011.645955, 2012b.

Lack, D. A., Bahreini, R., Langridge, J. M., Gilman, J. B., and Middlebrook, A. M.: Brown carbon absorption linked to organic mass tracers in biomass burning particles, Atmos. Chem. Phys., 13, 2415-2422, https://doi.org/10.5194/acp-13-2415-2013, 2013.

Langridge, J. M., Richardson, M. S., Lack, D., Law, D., and Murphy, D. M.: Aircraft Instrument for Comprehensive Characterization of Aerosol Optical Properties, Part I: Wavelength-Dependent Optical Extinction and Its Relative Humidity Dependence Measured Using Cavity Ringdown Spectroscopy, Aerosol Science and Technology, 45, 1305-1318, https://doi.org/10.1080/02786826.2011.592745, 2011.

Laskin, A., Lin, P., Laskin, J., Fleming, L. T., and Nizkorodov, S.: Molecular Characterization of Atmospheric Brown Carbon, in: Multiphase Environmental Chemistry in the Atmosphere, ACS Symposium Series, 1299, American Chemical Society, 261-274, 2018.

Levin, E. J. T., McMeeking, G. R., Carrico, C. M., Mack, L. E., Kreidenweis, S. M., Wold, C. E., Moosmüller, H., Arnott, W. P., Hao, W. M., Collett, J. L., and Malm, W. C.: Biomass burning smoke aerosol properties measured during Fire Laboratory at Missoula Experiments (FLAME), Journal of Geophysical Research: Atmospheres, 115, D18210, https://doi.org/10.1029/2009JD013601, 2010.

Lim, C. Y., Hagan, D. H., Coggon, M. M., Koss, A. R., Sekimoto, K., De Gouw, J., Warneke, C., Cappa, C. D., and Kroll, J. H.: Secondary organic aerosol formation from biomass burning emissions, Atmos. Chem. Phys. Discuss., https://doi.org/10.5194/acp-2019-326, 2019.

Lin, P., Aiona, P. K., Li, Y., Shiraiwa, M., Laskin, J., Nizkorodov, S. A., and Laskin, A.: Molecular Characterization of Brown Carbon in Biomass Burning Aerosol Particles, Environmental Science & Technology, 50, 11815-11824, https://doi.org/10.1021/acs.est.6b03024, 2016.

Liu, D. T., Whitehead, J., Alfarra, M. R., Reyes-Villegas, E., Spracklen, D. V., Reddington, C. L., Kong, S. F., Williams, P. I., Ting, Y. C., Haslett, S., Taylor, J. W., Flynn, M. J., Morgan, W. T., McFiggans, G., Coe, H., and Allan, J. D.: Black-carbon absorption enhancement in the atmosphere determined by particle mixing state, Nat. Geosci., 10, 184-U132, https://doi.org/10.1038/ngeo2901, 2017.

Liu, S., Aiken, A. C., Arata, C., Dubey, M. K., Stockwell, C. E., Yokelson, R. J., Stone, E. A., Jayarathne, T., Robinson, A. L., DeMott, P. J., and Kreidenweis, S. M.: Aerosol single scattering albedo dependence on biomass combustion efficiency: Laboratory and field studies, Geophysical Research Letters, 2013GL058392, https://doi.org/10.1002/2013GL058392, 2013.

Liu, S., Aiken, A. C., Gorkowski, K., Dubey, M. K., Cappa, C. D., Williams, L. R., Herndon, S. C., Massoli, P., Fortner, E. C., Chhabra, P. S., Brooks, W. A., Onasch, T. B., Worsnop, D. R., China, S., Sharma, N., Mazzoleni, C., Xu, L., L., N. N., Liu, D., Allan, J. D., Lee, J. D., Fleming, Z. L., Mohr, C., Zotter, P., Szidat, S., and Prevot, A. S. H.: Enhanced light absorption by mixed source black and brown carbon particles in UK winter, Nat. Comm., 6, 8435, https://doi.org/10.1038/ncomms9435, 2015.

Mann, G. W., Carslaw, K. S., Reddington, C. L., Pringle, K. J., Schulz, M., Asmi, A., Spracklen, D. V., Ridley, D. A., Woodhouse, M. T., Lee, L. A., Zhang, K., Ghan, S. J., Easter, R. C., Liu, X., Stier, P., Lee, Y. H., Adams, P. J., Tost, H., Lelieveld, J., Bauer, S. E., Tsigaridis, K., van Noije, T. P. C., Strunk, A., Vignati, E., Bellouin, N., Dalvi, M., Johnson, C. E., Bergman, T., Kokkola, H., von Salzen, K., Yu, F., Luo, G., Petzold, A., Heintzenberg, J., Clarke, A., Ogren, J. A., Gras, J., Baltensperger, U., Kaminski, U., Jennings, S. G., O'Dowd, C. D., Harrison, R. M., Beddows, D. C. S., Kulmala, M., Viisanen, Y., Ulevicius, V., Mihalopoulos, N., Zdimal, V., Fiebig, M., Hansson, H. C., Swietlicki, E., and Henzing, J. S.: Intercomparison and evaluation of global aerosol microphysical properties among AeroCom models of a range of complexity, Atmos. Chem. Phys., 14, 4679-4713, https://doi.org/10.5194/acp-14-4679-2014, 2014.

May, A. A., McMeeking, G. R., Lee, T., Taylor, J. W., Craven, J. S., Burling, I., Sullivan, A. P., Akagi, S., Collett Jr., J. L., Flynn, M., Coe, H., Urbanski, S. P., Seinfeld, J. H., Yokelson, R. J., and Kreidenweis, S. M.: Aerosol emissions from prescribed fires in the United States: A synthesis

746   of laboratory and aircraft measurements, Journal of Geophysical Research: Atmospheres, 119,
747   11,826-811,849, https://doi.org/10.1002/2014JD021848, 2014.

748   McMeeking, G. R., Kreidenweis, S. M., Baker, S., Carrico, C. M., Chow, J. C., Collett, J. L., Hao,
749   W. M., Holden, A. S., Kirchstetter, T. W., Malm, W. C., Moosmüller, H., Sullivan, A. P., and
750   Wold, C. E.: Emissions of trace gases and aerosols during the open combustion of biomass in the
751   laboratory, Journal of Geophysical Research: Atmospheres, 114, D19210,
752   https://doi.org/10.1029/2009JD011836, 2009.

753   McMeeking, G. R., Fortner, E., Onasch, T. B., Taylor, J. W., Flynn, M., Coe, H., and Kreidenweis,
754   S. M.: Impacts of nonrefractory material on light absorption by aerosols emitted from biomass
755   burning, Journal of Geophysical Research: Atmospheres, 119, 12,272-212,286,
756   https://doi.org/10.1002/2014JD021750, 2014.

757   Metcalf, A. R., Loza, C. L., Coggon, M. M., Craven, J. S., Jonsson, H. H., Flagan, R. C., and
758   Seinfeld, J. H.: Secondary Organic Aerosol Coating Formation and Evaporation: Chamber Studies
759   Using Black Carbon Seed Aerosol and the Single-Particle Soot Photometer, Aerosol Sci. Technol.,
760   47, 326-347, https://doi.org/10.1080/02786826.2012.750712, 2013.

761   Mohr, C., Lopez-Hilfiker, F. D., Zotter, P., Prévôt, A. S. H., Xu, L., Ng, N. L., Herndon, S. C.,
762   Williams, L. R., Franklin, J. P., Zahniser, M. S., Worsnop, D. R., Knighton, W. B., Aiken, A. C.,
763   Gorkowski, K. J., Dubey, M. K., Allan, J. D., and Thornton, J. A.: Contribution of Nitrated Phenols
764   to Wood Burning Brown Carbon Light Absorption in Detling, United Kingdom during Winter
765   Time, Environmental Science & Technology, 47, 6316-6324, https://doi.org/10.1021/es400683v,
766   2013.

767   Onasch, T. B., Trimborn, A. M., Fortner, E. C., Jayne, J. T., Kok, G. L., Williams, L. R.,
768   Davidovits, P., and Worsnop, D. R.: Soot Particle Aerosol Mass Spectrometer: Development,
769   Validation and Initial Application, Aerosol Science and Technology, 46, 804-817,
770   https://doi.org/10.1080/02786826.2012.663948, 2012.

771   Peng, J., Hu, M., Guo, S., Du, Z., Zheng, J., Shang, D., Zamora, M. L., Zeng, L., Shao, M., Wu,
772   Y.-S., Zheng, J., Wang, Y., Glen, C. R., Collins, D. R., Molina, M. J., and Zhang, R.: Markedly
773   enhanced absorption and direct radiative forcing of black carbon under polluted urban
774   environments, Proc. Natl. Acad. Sci. U. S. A., 113, 4266-4271,
775   https://doi.org/10.1073/pnas.1602310113, 2016.

776   Phillips, S. M., and Smith, G. D.: Spectroscopic comparison of water- and methanol-soluble brown
777   carbon particulate matter, Aerosol Science and Technology, 51, 1113-1121,
778   https://doi.org/10.1080/02786826.2017.1334109, 2017.

779   Pokhrel, R. P., Wagner, N. L., Langridge, J. M., Lack, D. A., Jayarathne, T., Stone, E. A.,
780   Stockwell, C. E., Yokelson, R. J., and Murphy, S. M.: Parameterization of single-scattering albedo
781   (SSA) and absorption Ångström exponent (AAE) with EC / OC for aerosol emissions from
782   biomass burning, Atmos. Chem. Phys., 16, 9549-9561, https://doi.org/10.5194/acp-16-9549-2016,
783   2016.

784   Pokhrel, R. P., Beamesderfer, E. R., Wagner, N. L., Langridge, J. M., Lack, D. A., Jayarathne, T.,
785   Stone, E. A., Stockwell, C. E., Yokelson, R. J., and Murphy, S. M.: Relative importance of black
786   carbon, brown carbon, and absorption enhancement from clear coatings in biomass burning
787   emissions, Atmospheric Chemistry and Physics, 17, 5063-5078, https://doi.org/10.5194/acp-17-
788   5063-2017, 2017.

Qin, Y. M., Tan, H. B., Li, Y. J., Li, Z. J., Schurman, M. I., Liu, L., Wu, C., and Chan, C. K.: Chemical characteristics of brown carbon in atmospheric particles at a suburban site near Guangzhou, China, Atmos. Chem. Phys., 18, 16409-16418, https://doi.org/10.5194/acp-18-16409-2018, 2018.

Reid, J. S., Koppmann, R., Eck, T. F., and Eleuterio, D. P.: A review of biomass burning emissions part II: intensive physical properties of biomass burning particles, Atmos. Chem. Phys., 5, 799-825, https://doi.org/10.5194/acp-5-799-2005, 2005.

Sahu, L. K., Kondo, Y., Moteki, N., Takegawa, N., Zhao, Y., Cubison, M. J., Jimenez, J. L., Vay, S., Diskin, G. S., Wisthaler, A., Mikoviny, T., Huey, L. G., Weinheimer, A. J., and Knapp, D. J.: Emission characteristics of black carbon in anthropogenic and biomass burning plumes over California during ARCTAS-CARB 2008, Journal of Geophysical Research-Atmospheres, 117, https://doi.org/10.1029/2011jd017401, 2012.

Saleh, R., Hennigan, C. J., McMeeking, G. R., Chuang, W. K., Robinson, E. S., Coe, H., Donahue, N. M., and Robinson, A. L.: Absorptivity of brown carbon in fresh and photo-chemically aged biomass-burning emissions, Atmospheric Chemistry and Physics, 13, 7683-7693, https://doi.org/10.5194/acp-13-7683-2013, 2013.

Saleh, R., Robinson, E. S., Tkacik, D. S., Ahern, A. T., Liu, S., Aiken, A. C., Sullivan, R. C., Presto, A. A., Dubey, M. K., Yokelson, R. J., Donahue, N. M., and Robinson, A. L.: Brownness of organics in aerosols from biomass burning linked to their black carbon content, Nature Geosci, 7, 647-650, https://doi.org/10.1038/ngeo2220, 2014.

Saleh, R., Cheng, Z., and Atwi, K.: The Brown–Black Continuum of Light-Absorbing Combustion Aerosols, Environmental Science & Technology Letters, ASAP, https://doi.org/10.1021/acs.estlett.8b00305, 2018.

Schneider, J., Weimer, S., Drewnick, F., Borrmann, S., Helas, G., Gwaze, P., Schmid, O., Andreae, M. O., and Kirchner, U.: Mass spectrometric analysis and aerodynamic properties of various types of combustion-related aerosol particles, International Journal of Mass Spectrometry, 258, 37-49, https://doi.org/10.1016/j.ijms.2006.07.008, 2006.

Schwarz, J. P., Gao, R. S., Spackman, J. R., Watts, L. A., Thomson, D. S., Fahey, D. W., Ryerson, T. B., Peischl, J., Holloway, J. S., Trainer, M., Frost, G. J., Baynard, T., Lack, D. A., de Gouw, J. A., Warneke, C., and Del Negro, L. A.: Measurement of the mixing state, mass, and optical size of individual black carbon particles in urban and biomass burning emissions, Geophysical Research Letters, 35, L13810, https://doi.org/10.1029/2008gl033968, 2008.

Sekimoto, K., Koss, A. R., Gilman, J. B., Selimovic, V., Coggon, M. M., Zarzana, K. J., Yuan, B., Lerner, B. M., Brown, S. S., Warneke, C., Yokelson, R. J., Roberts, J. M., and de Gouw, J.: High- and low-temperature pyrolysis profiles describe volatile organic compound emissions from western US wildfire fuels, Atmos. Chem. Phys., 18, 9263-9281, https://doi.org/10.5194/acp-18-9263-2018, 2018.

Sengupta, D., Samburova, V., Bhattarai, C., Kirillova, E., Mazzoleni, L., Iaukea-Lum, M., Watts, A., Moosmüller, H., and Khlystov, A.: Light absorption by polar and non-polar aerosol compounds from laboratory biomass combustion, Atmos. Chem. Phys., 18, 10849-10867, https://doi.org/10.5194/acp-18-10849-2018, 2018.

830 Shamjad, P. M., Tripathi, S. N., Thamban, N. M., and Vreeland, H.: Refractive Index and
831 Absorption Attribution of Highly Absorbing Brown Carbon Aerosols from an Urban Indian City-
832 Kanpur, Scientific Reports, 6, 37735, https://doi.org/10.1038/srep37735, 2016.

833 Shiraiwa, M., Kondo, Y., Iwamoto, T., and Kita, K.: Amplification of Light Absorption of Black
834 Carbon by Organic Coating, Aerosol Science and Technology, 44, 46-54,
835 https://doi.org/10.1080/02786820903357686, 2010.

836 Sumlin, B. J., Pandey, A., Walker, M. J., Pattison, R. S., Williams, B. J., and Chakrabarty, R. K.:
837 Atmospheric Photooxidation Diminishes Light Absorption by Primary Brown Carbon Aerosol
838 from Biomass Burning, Environmental Science & Technology Letters, 4, 540-545,
839 https://doi.org/10.1021/acs.estlett.7b00393, 2017.

840 Sumlin, B. J., Heinson, Y. W., Shetty, N., Pandey, A., Pattison, R. S., Baker, S., Hao, W. M., and
841 Chakrabarty, R. K.: UV–Vis–IR spectral complex refractive indices and optical properties of
842 brown carbon aerosol from biomass burning, Journal of Quantitative Spectroscopy and Radiative
843 Transfer, 206, 392-398, https://doi.org/10.1016/j.jqsrt.2017.12.009, 2018.

844 Wandinger, Ulla, Müller, Detlef, Böckmann, Christine, Althausen, Dietrich, Matthias, Volker,
845 Bösenberg, Jens, Weiß, Volker, Fiebig, Markus, Wendisch, Manfred, Stohl, Andreas, and
846 Ansmann, A.: Optical and microphysical characterization of biomass- burning and industrial-
847 pollution aerosols from- multiwavelength lidar and aircraft measurements, Journal of Geophysical
848 Research: Atmospheres, 107, LAC 7-1-LAC 7-20, https://doi.org/doi:10.1029/2000JD000202,
849 2002.

850 Washenfelder, R. A., Attwood, A. R., Brock, C. A., Guo, H., Xu, L., Weber, R. J., Ng, N. L., Allen,
851 H. M., Ayres, B. R., Baumann, K., Cohen, R. C., Draper, D. C., Duffey, K. C., Edgerton, E., Fry,
852 J. L., Hu, W. W., Jimenez, J. L., Palm, B. B., Romer, P., Stone, E. A., Wooldridge, P. J., and
853 Brown, S. S.: Biomass burning dominates brown carbon absorption in the rural southeastern
854 United States, Geophysical Research Letters, 42, 653-664,
855 https://doi.org/10.1002/2014GL062444, 2015.

856 Xie, M., Hays, M. D., and Holder, A. L.: Light-absorbing organic carbon from prescribed and
857 laboratory biomass burning and gasoline vehicle emissions, Scientific Reports, 7, 7318,
858 https://doi.org/10.1038/s41598-017-06981-8, 2017.

859 Yang, M., Howell, S. G., Zhuang, J., and Huebert, B. J.: Attribution of aerosol light absorption to
860 black carbon, brown carbon, and dust in China – interpretations of atmospheric measurements
861 during EAST-AIRE, Atmospheric Chemistry and Physics, 9, 2035-2050,
862 https://doi.org/10.5194/acp-9-2035-2009, 2009.

863 Zhang, X., Kim, H., Parworth, C., Young, D. E., Zhang, Q., Metcalf, A. R., and Cappa, C. D.:
864 Optical Properties of Wintertime Aerosols from Residential Wood Burning in Fresno, CA: Results
865 from DISCOVER-AQ 2013, Environmental Science & Technology, 50, 1681-1690,
866 https://doi.org/10.1021/acs.est.5b04134, 2016.

867

868

869

9 Tables

Table 1. Fuels by particle Class.

Class	Fuel	SSA range	[OA]/[BC] range
Class 1	Chaparral, canopy, litter (pine), building materials, excelsior	0.23-0.43	0.3-2.4
Class 2	Manzanita, Sage, litter (fir)	0.43-0.60	1.5-4.1
Type 3	Pine, fir, litter, canopy, juniper	0.60-0.74	6.6-20
Class 4	Pine, fir, canopy, rotten log, ceonothos	0.74-0.87	8.3-55
Class 5	Canopy (pine), rice, bear grass, duff	0.87-0.93	31-143
Class 6	Rotten log, duff, peat, dung	0.93-1.00	$431-10^5$

872

873

10 Figures

875
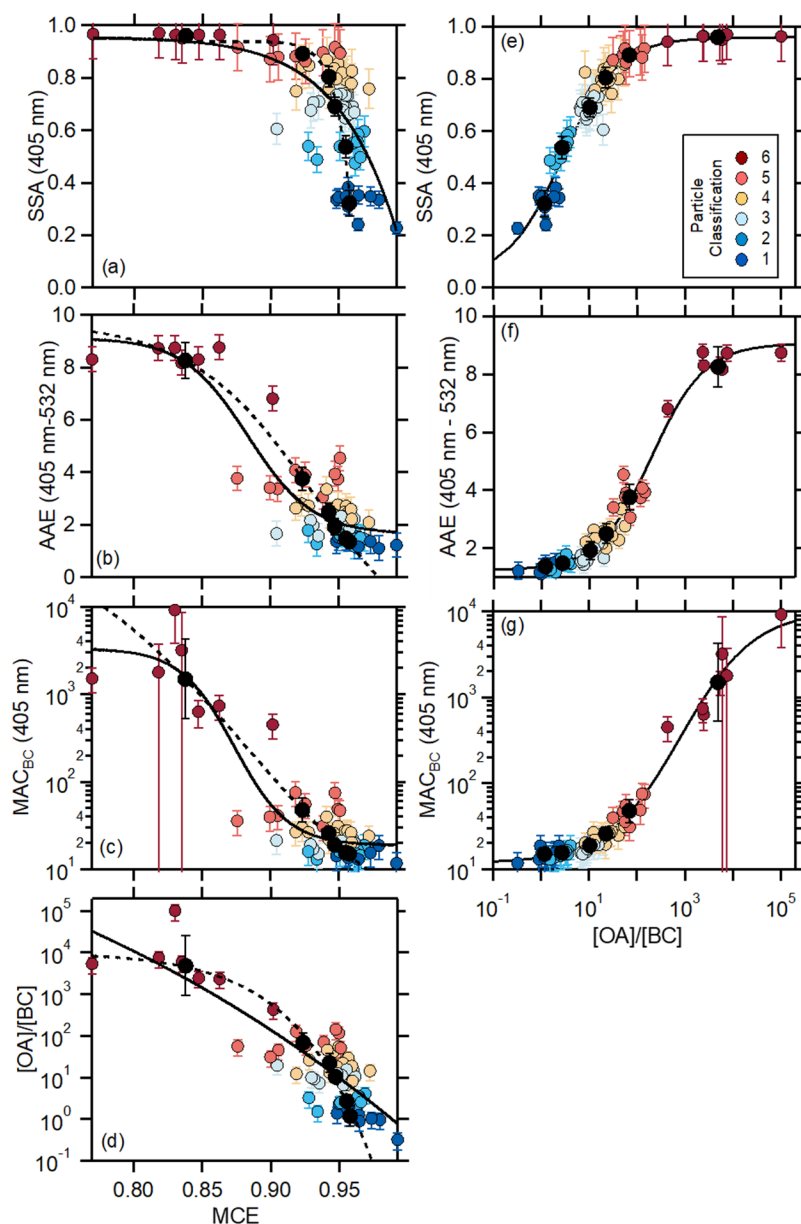
Figure 1. (left panels) Relationship between (a) the SSA_{405nm}, (b) the $AAE_{405-532}$, (c) the MAC_{BC}, and (d) the [OA]/[BC] mass ratio and the modified combustion efficiency, MCE. Results for individual burns are shown as points colored by the particle Class, and Class average values are shown as black circles. Uncertainties on the Class averages are 1σ based on measurement variability and uncertainties on for the individual burns are from error propagation of measurement uncertainties. The solid black lines are fits to the individual burns (colored points) while the dashed black lines are fits to the Class averages (Table S2). (right panels) Relationship between (e) the SSA_{405nm}, (f) the $AAE_{405-532}$, and (g) the MAC_{BC} on the [OA]/[BC] mass ratio. The solid black lines here are sigmoidal fits to the individual burns. Fits to the Class averages are similar.

886
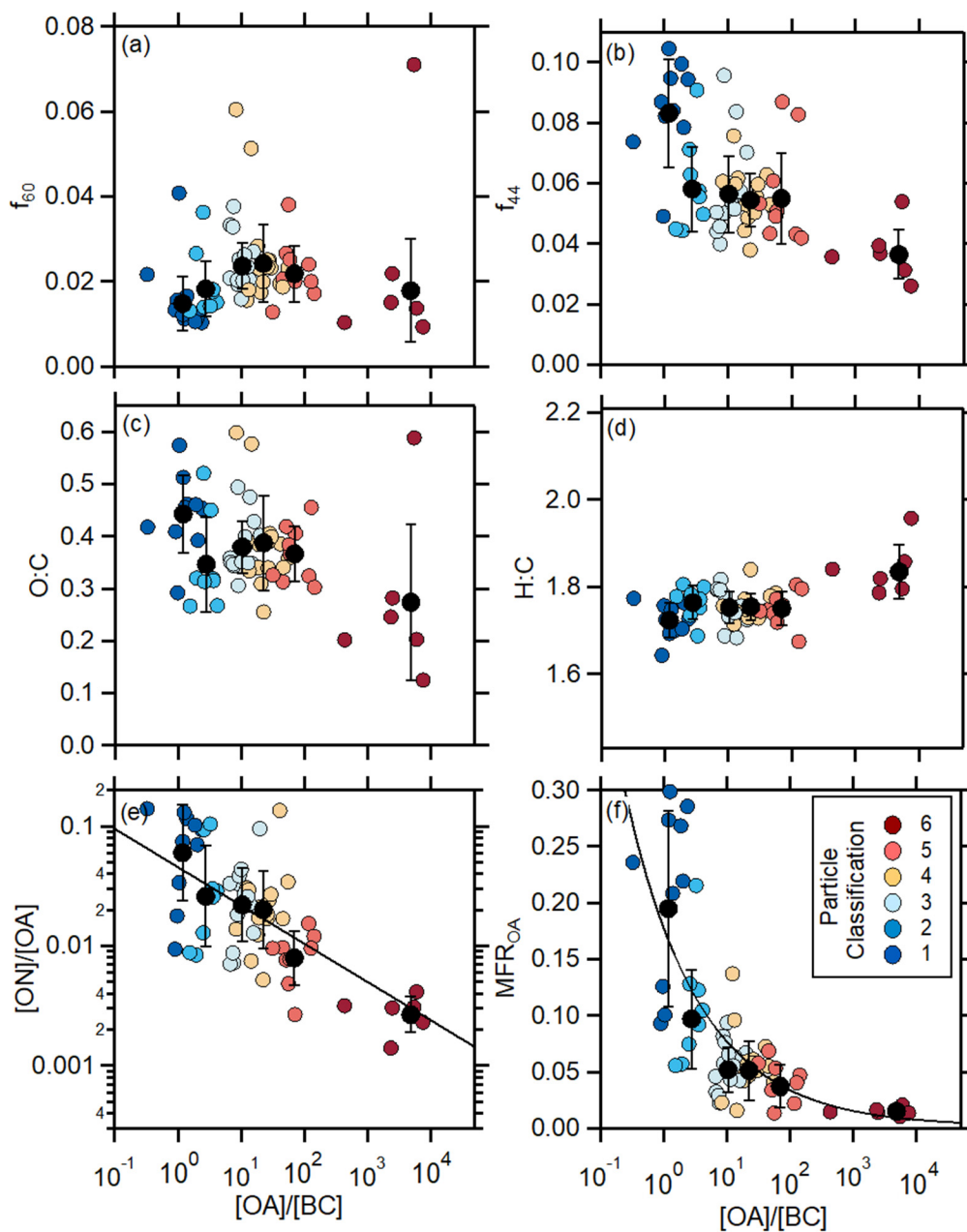
Figure 2. Dependence of (a) f_{60}, (b) f_{44}, (c) O:C, (d) H:C, (e) the nitrated organic fraction of OA, f_{ON-OA}, and (f) the OA volatility, characterized as the mass fraction remaining after heating. Results for individual burns are shown as points colored by the particle Class, and Class average values are shown as black circles. Uncertainties on the Class averages are 1σ based on measurement variability. For f_{ON-OA} and MFR_{OA}, fits to the observations are shown (see text).

892

893
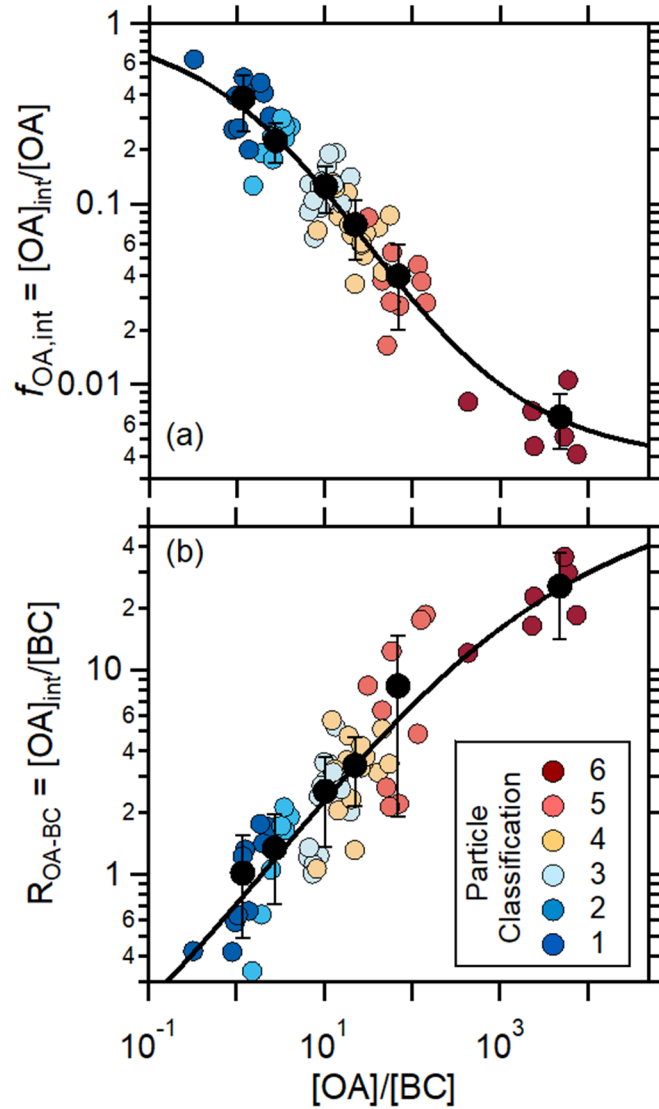
Figure 3. Relationship between (a) the fraction of OA that is internally mixed with BC, $f_{OA,int}$ and (b) the OA-to-BC mass ratio for only the internally mixed OA, and the total [OA]/[BC] mass ratio. Results for individual burns are shown as points colored by the particle Class, and Class average values are shown as black circles. Uncertainties on the Class averages are 1σ based on measurement variability. Black lines are sigmoidal fits to the data, in log-log space.

899
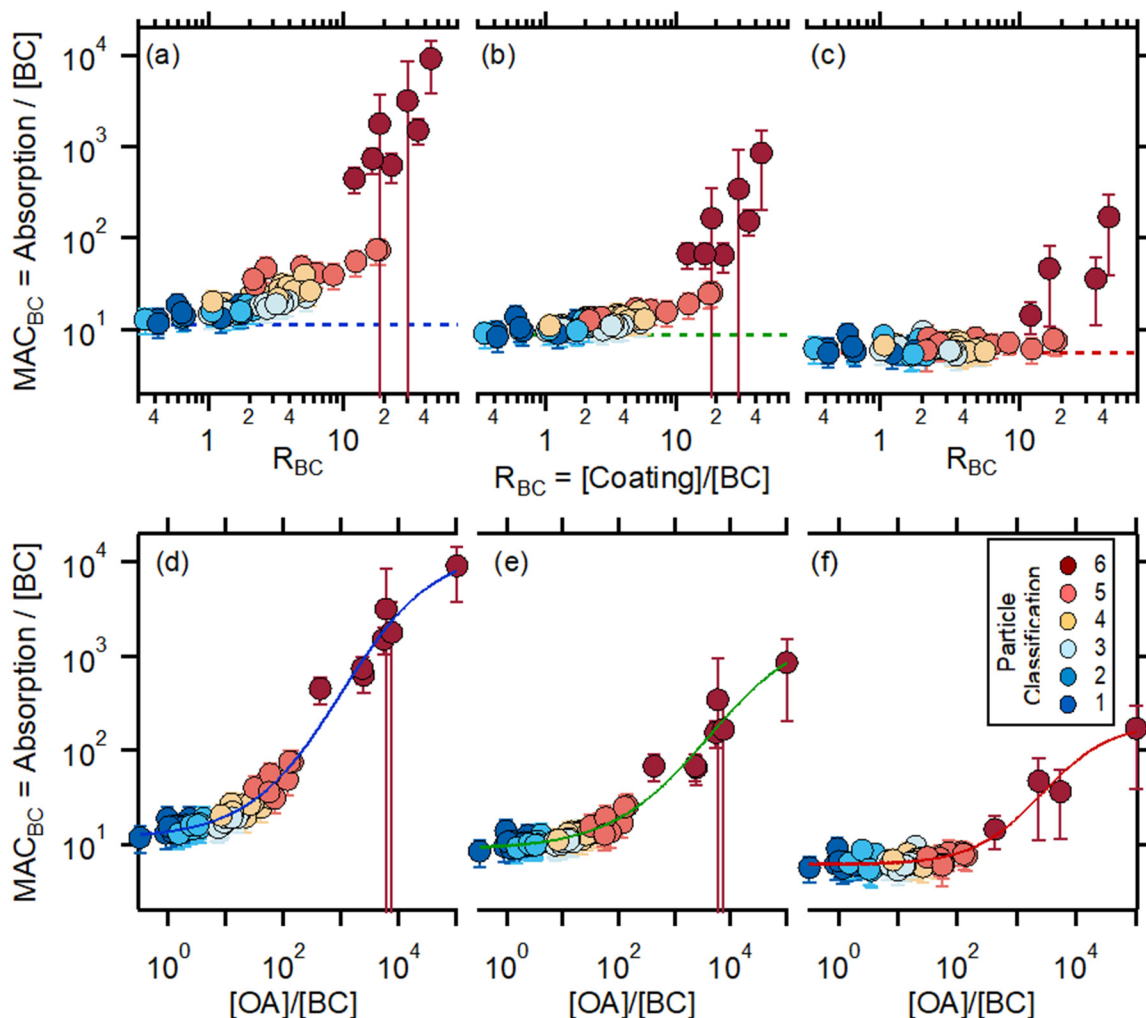
Figure 4. (Top Panels) The relationship between the wavelength-specific MAC_{BC} and the coating-to-BC mass ratio for (a) 405 nm, (b) 532 nm and (c) 781 nm. The horizontal dashed lines show the derived $MAC_{BC,pure}$ values. (Bottom Panels) The relationship between the wavelength-dependent MAC_{BC} and the total [OA]/[BC] mass ratio for (d) 405 nm, (e) 532 nm and (f) 781 nm. The lines are sigmoidal fits. Uncertainties for the individual burns are determined from error propagation. Graphs of the wavelength-specific MAC_{BC} versus [OA]/[BC] with each shown using independent y-axis scales are provided for comparison in **Figure S1**.

909
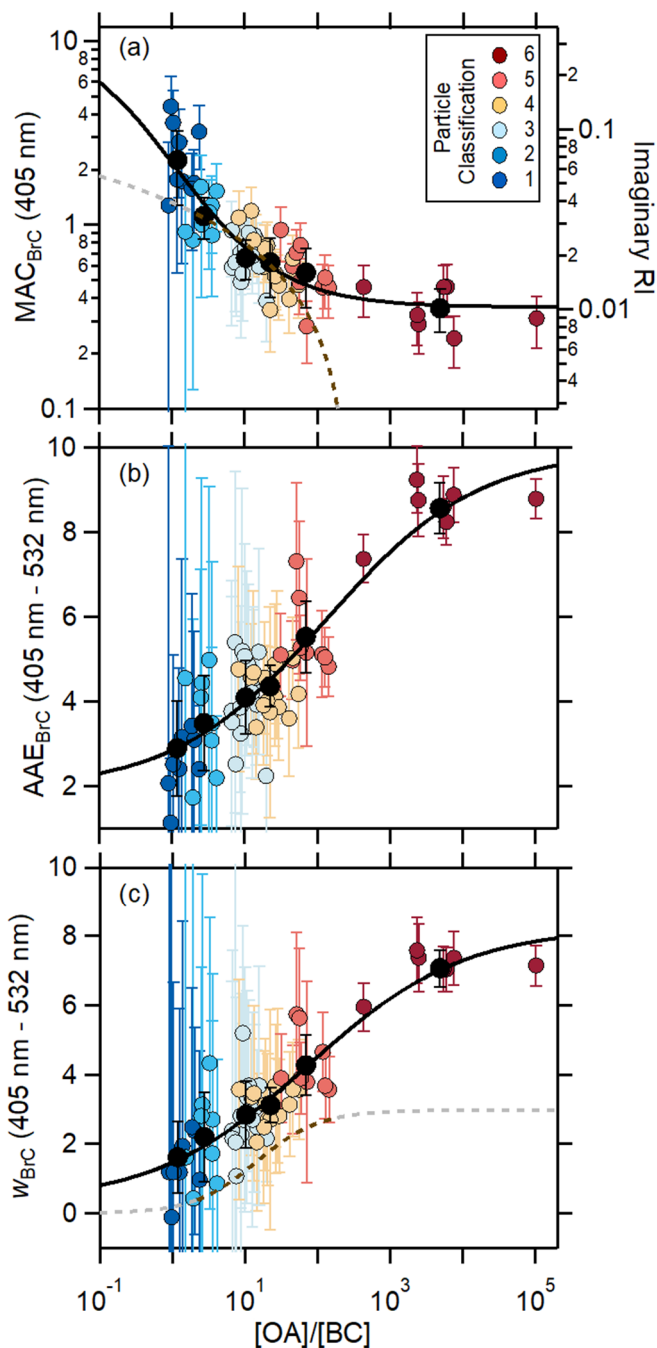
Figure 5. Relationship between (a) $MAC_{BrC,405nm}$, (b) $AAE_{BrC,405-532}$, and (c) $w_{BrC,405-532}$ and the [OA]/[BC] mass ratio. The solid lines are sigmoidal fits to the observations, against log([OA]/[BC]). The dashed lines are based on the parameterization of Saleh et al. (2014), with the brown color indicating the measuring range in that study and the gray color extrapolated. Results for individual burns are shown as points colored by the particle Class, and Class average values are shown as black circles. Uncertainties on the Class averages are 1σ based on measurement variability. Uncertainties for the individual burns are determined from error propagation.

918

919
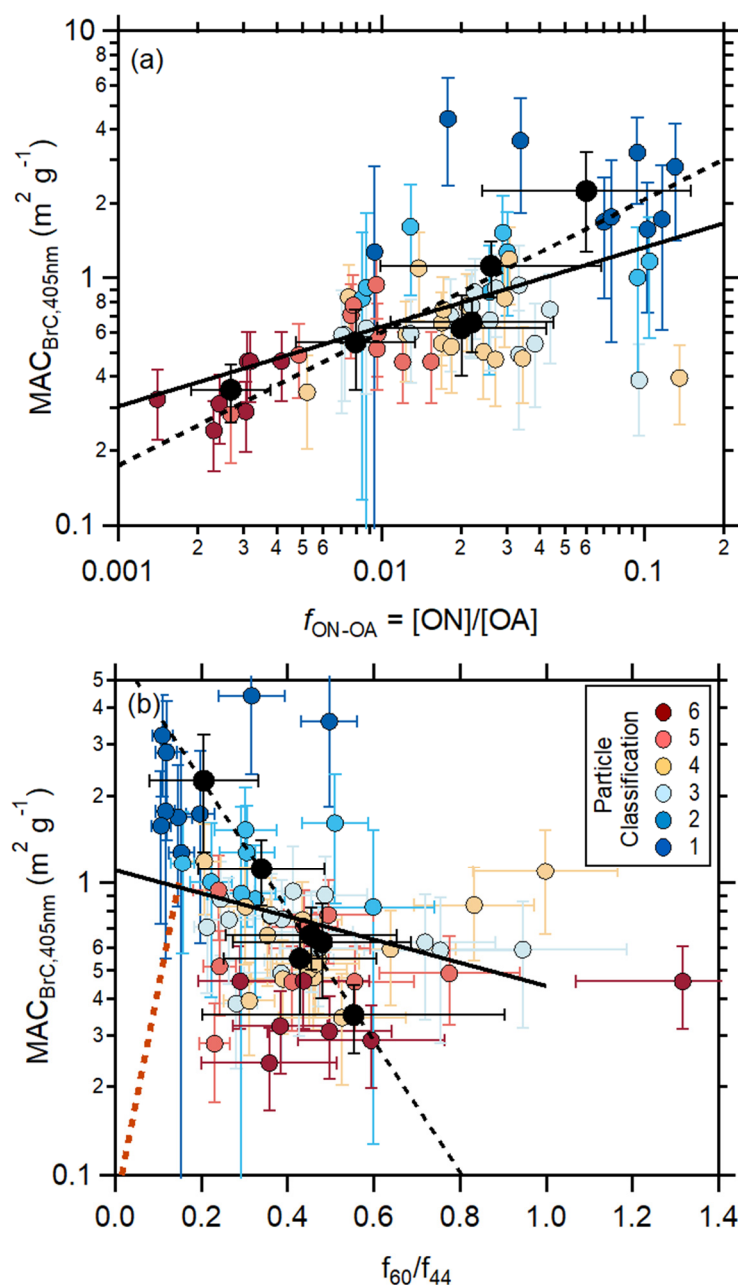
Figure 6. Relationship between the $MAC_{BrC,405nm}$ and (a) the nitrated organic fraction of total organic aerosol, f_{ON-OA}, and (b) the f_{60}/f_{44} ion ratio for organic aerosol. Results for individual burns are shown as points colored by the particle Class, and Class average values are shown as black circles. Uncertainties on the Class averages are 1σ based on measurement variability. Uncertainties for the individual burns are determined from error propagation. Solid black lines are fits to all burns and dashed black lines are fits to the Class averages. The dashed brown line in panel (b) is the relationship reported by Lack et al. (2013) for ambient particles in a biomass burning plume.

927

928
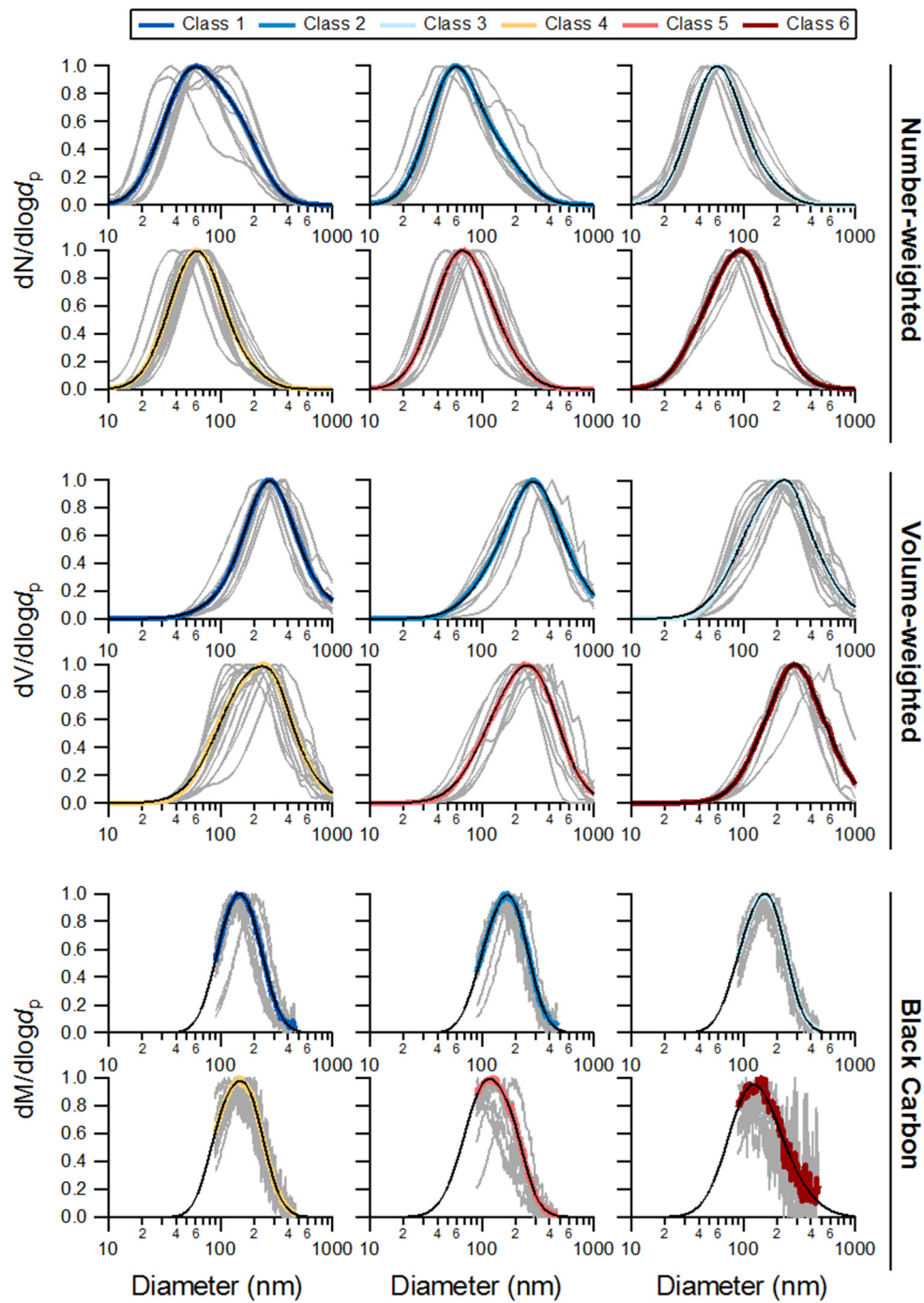
Figure 7. Class-specific total particle number-weighted (top) and volume-weighted (middle) mobility size distributions, and the BC-only mass-weighted (bottom) size distribution. Individual burns are shown in gray and class averages are shown as colors. Bimodal log-normal fits are thin black lines. Note that the number-weighted and volume-weighted distributions are graphed versus mobility diameter and the BC mass-weighted distribution against the BC volume equivalent diameter.

935
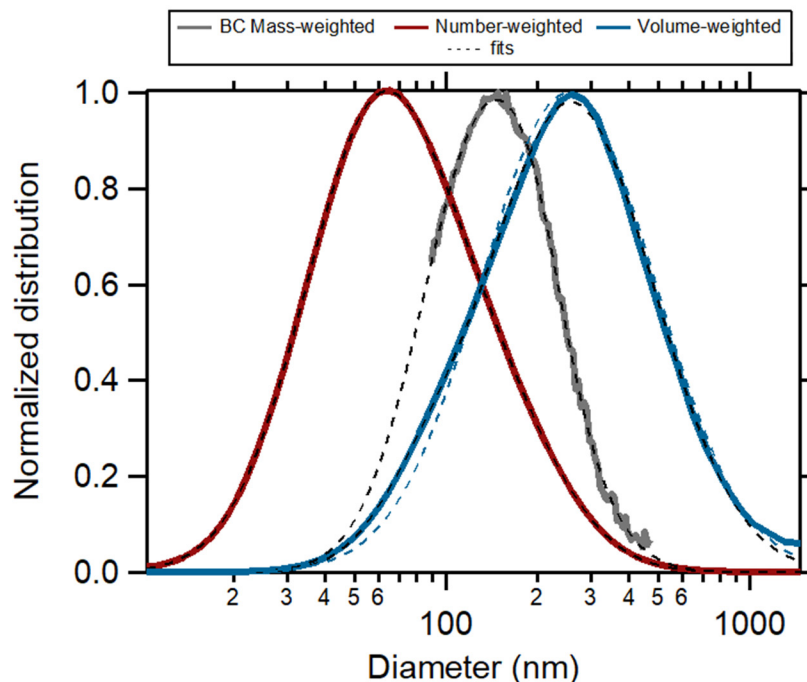
Figure 8. Average total particle number-weighted (red) and volume-weighted (blue) size
distributions and the BC-specific mass-weighted size distributions. Black dashed lines are bimodal
log-normal fits. The dashed blue line is the total particle volume-weighted distribution calculated
from a single-mode fit to the number-weighted distribution. Note that the number-weighted and
volume-weighted distributions are graphed versus mobility diameter and the BC mass-weighted
distribution against the BC volume equivalent diameter.

942

943
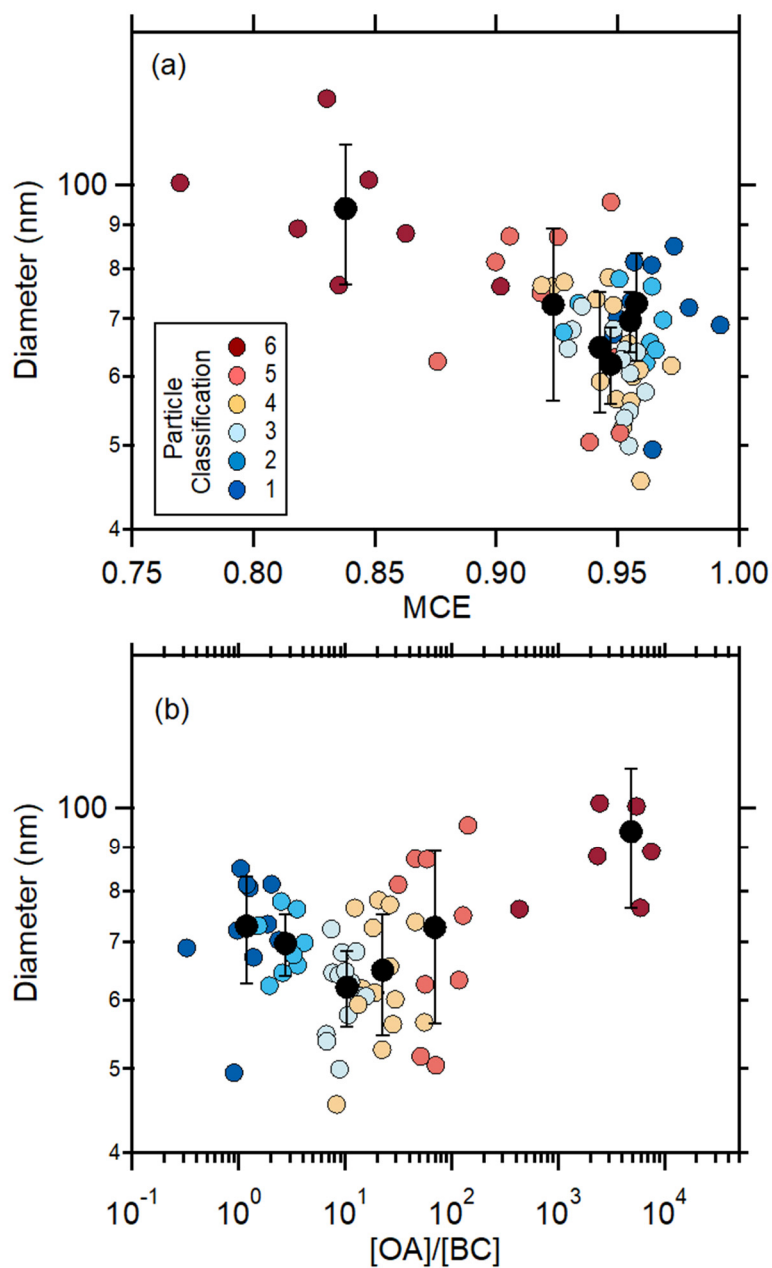
Figure 9. Relationship between number-weighted particle median diameter and (a) the MCE and (b) the [OA]/[BC] ratio. Colored circles are for individual burns and black circles for particle class averages.

947
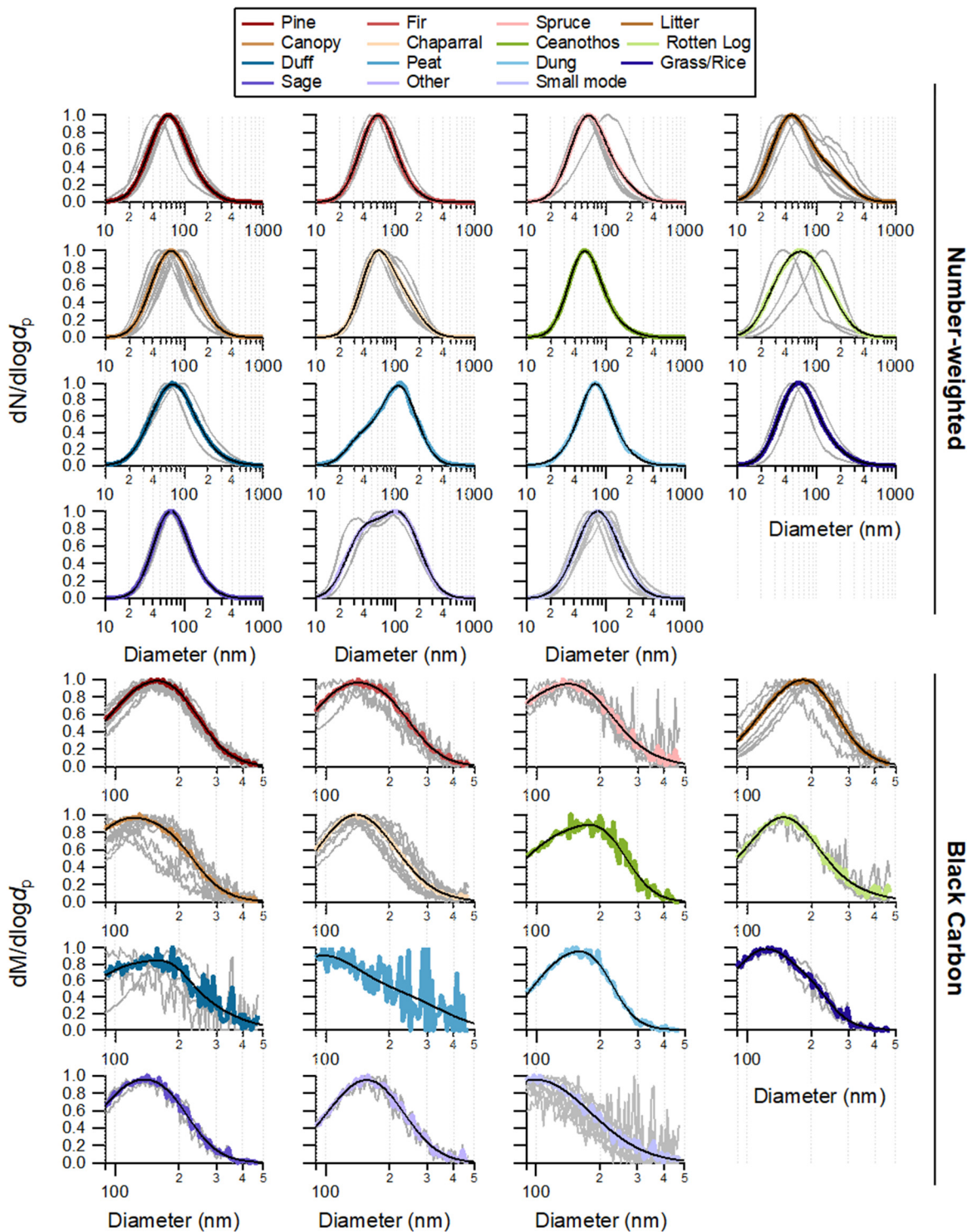
Figure 10. Normalized total particle number-weighted (top) and the BC-only mass-weighted (bottom) size distributions shown by fuel type (see legend). Individual burns are gray and averages for a fuel type colors. For some fuels there is only one size distribution. Bimodal log-normal fits are the black lines. The "other" category includes non-traditional biofuels, specifically building materials and excelsior.